INVESTIGATION OF HYDROGEN AND ITS ROLE IN DEHYDRATION PROCESSES IN HALLOYSITE

A THESIS

Presented to

The Faculty of the Graduate Division

by

Billy Banks Harris, Jr.

In Partial Fulfillment

of the Requirements for the Degree

Master of Science in Ceramic Engineering

Georgia Institute of Technology

March, 1971

In presenting the dissertation as a partial fulfillment of the requirements for an advanced degree from the Georgia Institute of Technology, I agree that the Library of the Institute shall make it available for inspection and circulation in accordance with its regulations governing materials of this type. I agree that permission to copy from, or to publish from, this dissertation may be granted by the professor under whose direction it was written, or, in his absence, by the Dean of the Graduate Division when such copying or publication is solely for scholarly purposes and does not involve potential financial gain. It is understood that any copying from, or publication of, this dissertation which involves potential financial gain will not be allowed without written permission.

7/25/68

INVESTIGATION OF HYDROGEN AND ITS ROLE IN DEHYDRATION PROCESSES IN HALLOYSITE

Approved: [redacted]

Date approved by Chairman: [redacted]

ACKNOWLEDGMENTS

I am greatly indebted to my principal advisor, Dr. Stephen Spooner, whose sincere interest and enthusiasm was second only to his constructive guidance.

I would like to thank Dr. J. F. Benzel and Dr. Lane Mitchell for their participation as members of my thesis advisory committee.

I wish to thank the staff of the Georgia Tech Research Reactor and the Neutron Diffraction Group for their cooperation and willingness to help, and for the use of their facilities.

I am also indebted to Dr. Reiner J. Gerdes and to Mr. Thomas H. B. Sanders for their help with instrumentation and procedures.

Finally, I wish to thank my wife and parents for their encouragement during this work.

TABLE OF CONTENTS

TABLE OF CONTENTS (Concluded)

LIST OF TABLES

LIST OF FIGURES

LIST OF FIGURES (Concluded)

SUMMARY

The dehydration of hydrated halloysite from Chattooga County, Georgia was investigated. Specimen characterization was accomplished by x-ray diffraction, x-ray fluorescence spectroscopy, electron microscopy, crystallite size determination, and thermal analyses. The tubular morphology was confirmed by scanning electron microscopy.

The decrease in the (001) plane spacing from 10.1 to 7.4 Å is associated with an interlayer water loss and was observed by x-ray diffraction. Also associated with dehydration is the appearance of an (002) reflection that is not observed in hydrated halloysite. X-ray diffraction patterns indicated that no further changes occurred upon heating to 300°C.

Neutron diffraction patterns confirmed structural changes as observed by shifts in basal reflections. The diffuse background in neutron scattering patterns dropped sharply as the sample was heated to higher temperatures. After making suitable corrections, it was found that the diffuse background was a quantitative indication of the hydrogen content.

The utilization of a standard scatterer afforded a means to calculate quantitatively the hydrogen loss after heating to several temperatures up to 300°C. Hydrogen loss was converted to percent water loss for comparison to thermal gravimetric analysis weight loss. Higher values of weight loss as obtained by neutron scattering were attributed primarily to the extended time of heat treatment; the possibility that bonded water loss or loss of structural hydrogen may begin at lower temperatures than previously reported was suggested.

CHAPTER I

INTRODUCTION

Halloysite, a clay mineral of the kaolinite group, was formerly used in the manufacture of dentures and for the production of alum. Concerning ceramic applications, halloysite bodies, when fired to high temperatures, develop small cracks which are detrimental to the strength and appearance of the finished product. Pure halloysite is not usually found in abundant quantities, but is combined as a contaminant in other clays or with metal oxides (usually iron or manganese). Many hard kaolins were mistakenly called halloysite before the development of x-ray diffraction techniques; even after x-ray analysis became a common method of structural and mineralogical analysis, it is probable that halloysite was often identified as kaolinite. Halloysite is probably interspersed in many kaolinite bodies, but is rarely detected; up to 60 percent halloysite can easily be overlooked in x-ray diffraction patterns.

The nomenclature associated with halloysite has been confusing. European and American mineralogists have adopted several terms, including endellite and metahalloysite. For the purposes of this research, the term halloysite is used to describe the mineral $Al_2O_3 \cdot 2SiO_2 \cdot 2\ H_2O$, and hydrated halloysite to describe $Al_2O_3 \cdot 2SiO_2 \cdot 4\ H_2O$.

Before the development of x-ray diffraction techniques, halloysite was regarded as essentially amorphous. It is now known to be a modification of the kaolinite structure, apparently containing the basic kaolinite

unit cell with water molecules interleaved between layers. The individual layers overcome the strain induced by a slight misfit by curling at the edges. Water can help bind the layers together, so that a tubular crystal is formed. Upon heating, interlayer water is lost, and the tubes frequently split and unroll. Such a morphology gives rise to two-dimensional lattice effects.

The x-ray diffraction pattern of halloysite shows broad peaks corresponding to (00ℓ) reflections, implying an irregular stacking sequence. Broad reflection regions caused by two-dimensional diffraction predominate, and detailed structure analyses cannot be made by conventional x-ray diffraction techniques.

It is the purpose of this research to study the irreversible dehydration process with emphasis on the loss of hydrogen as temperature is increased. Thermal gravimetric analysis is used to determine weight loss as a function of temperature. X-ray and neutron diffraction are used to study structural changes that occur upon heating. Neutron diffraction is also used to establish quantitatively the loss of hydrogen after hydrated halloysite has been heated to several temperatures. Loss of hydrogen can be directly observed as a reduction of the diffuse background in neutron diffraction patterns. Correlation of TGA and neutron diffraction data offers a method to postulate on the role of hydrogen in dehydration processes. Neutron scattering appears to offer a new means to study hydrogen loss quantitatively and to observe more clearly the dissimilarities in complex clay minerals related to hydrogen content.

CHAPTER II

BACKGROUND

The Structure of Halloysite

Early Investigations

Among the minerals described as kaolinite and halloysite, varieties exist which differ both in morphology and in the degree of structural order. "Kaolin mineral" is used as a general term to cover kaolinite, halloysite, dickite, nacrite, and intermediate forms.

Berthier (1) described and named halloysite in 1826, in honor of Omalius d'Halloy, who had observed the mineral in a district of old zinc and iron mines near Liège, Belgium. From that time until 1934 it was regarded as an amorphous substance with no characteristic crystalline structure. Mellor (2) in 1908 described halloysite in his review of amorphous materials. In 1934, Ross and Kerr (3) concluded from x-ray diffraction data that halloysite occupies a state of crystallinity between that of kaolinite and allophane.

Shaw and Humbert (4) in 1941 used electron microscopy to revise the early concepts of the morphology of halloysite, noting the presence of split rods and concluding that the structures proposed for halloysite do not explain its observed features.

In a detailed study in 1950, Bates, Hildebrand, and Swineford (5) found that halloysite exists in the form of hollow tubes, many of which are split longitudinally and collapsed to form laths or ribbons. Struc-

tural considerations led to the conclusion that halloysite crystals take the form of well-developed tubes, and that the strain produced by dehydration causes the tubes to collapse, split, and unroll. Their concept of the morphology is shown in Figure 1.

In its most characteristic form, halloysite consists of tubular or rolled particles, with considerable variations in size. Bates and Comer (6) determined that, for most species, the ratio of length to width lies in the range of three to six. In 1948, Brindley and Robinson (7) determined that the structural layers scatter x rays in a manner largely incoherent from layer to layer. This incoherent scattering results in a diffuse band on a powder photograph in the region where kaolinite gives definite lines.

Relationship Between Kaolinite and Halloysite

A basic question is where to draw the line between a disordered kaolinite and halloysite. Brindley, Santos, and Santos (8) in 1963 proposed that the names kaolinite and halloysite relate primarily to morphological varieties. A kaolinite flake which is beginning to curl or roll may or may not become a fully developed tube of the halloysite form. The term halloysite should be used as soon as a "significant" degree of curvature has developed. It is difficult to determine what a "significant" degree of curvature consists of, and herein lies the difficulty in distinguishing the boundary between kaolinite and halloysite. The layer structures of kaolinite and halloysite, after Brindley, are shown in Figure 2.

The distinction of degrees of curvature may not be satisfactory because plate forms of halloysite exist, disordered with respect to both the a- and b-axes; consequently, particles with a kaolinite morphology

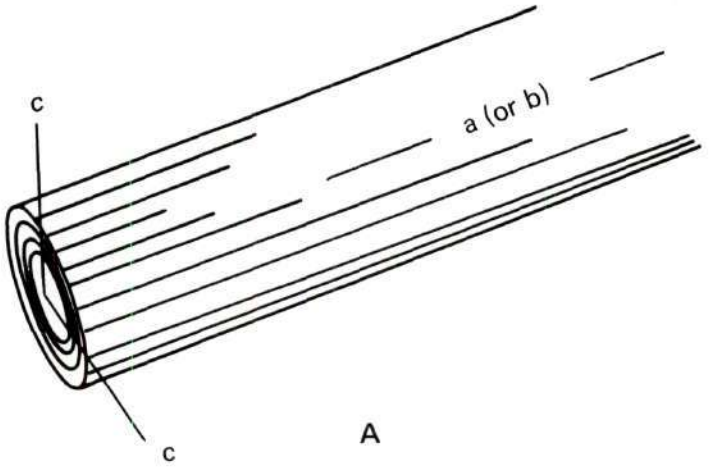

A

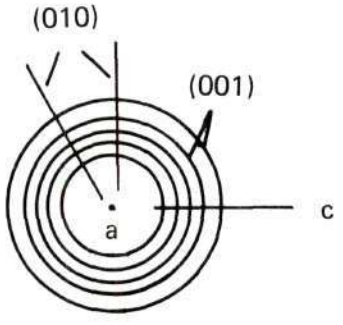

B

Figure 1. Relation of Morphology to Structure in Halloysite.
(A) Halloysite Tube
(B) Cross Section Showing Crystallographic Axes and Major Planes

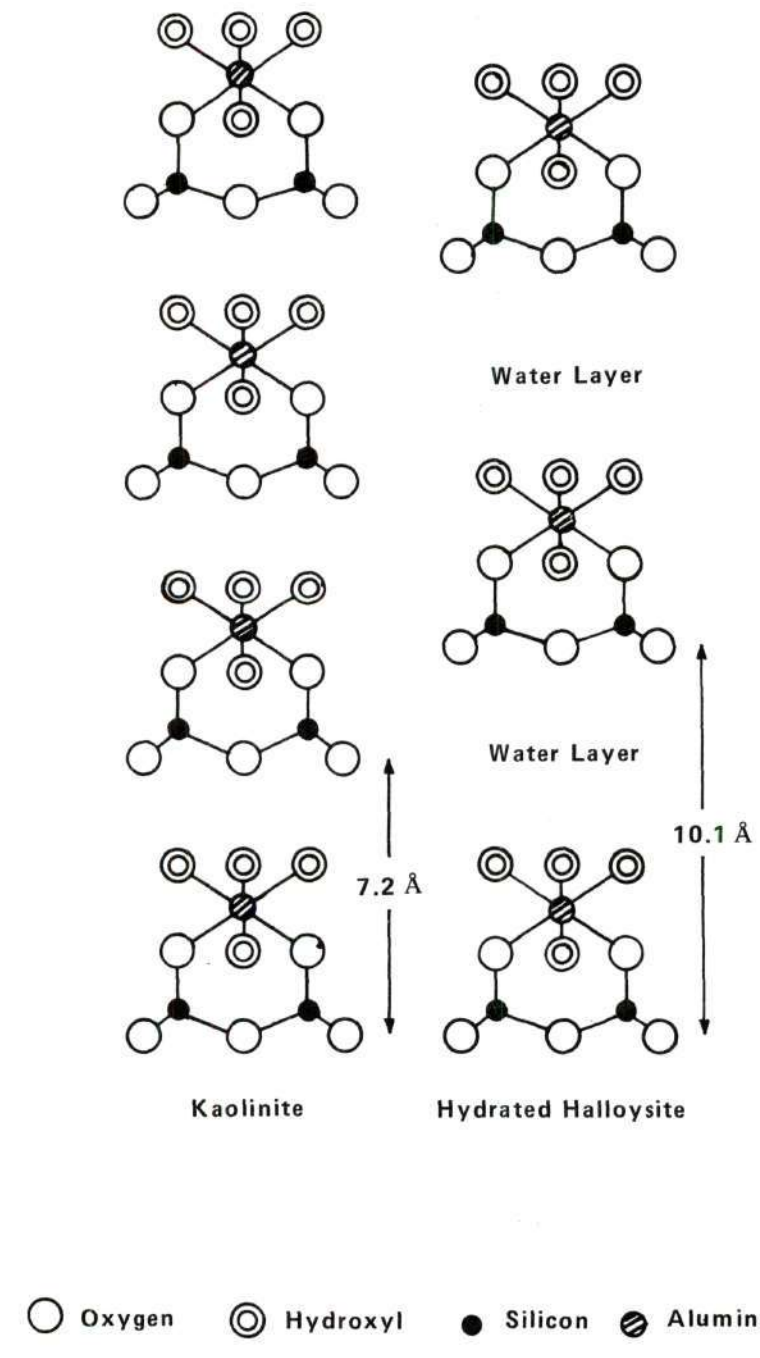

Figure 2. Layer Structure of Hydrated Halloysite and Kaolinite.

could have the x-ray characteristics of halloysite. Brindley, Santos, and Santos also studied various mixtures of kaolinite and halloysite by x-ray diffraction. The difficulty in making a distinction is illustrated in the series of diffraction patterns shown in Figure 3. Figure 3A shows the diffraction pattern of a well-crystallized kaolinite, and 3F a well-formed halloysite. Figures 3E and 3D exhibit barely noticeable changes, with five and ten percent kaolinite, respectively. Figure 3C resembles the pattern of a disordered kaolinite with a lack of basal enhancement. With 40 percent kaolinite, Figure 3B, the material appears to be a slightly disordered kaolinite, i.e., 60 percent halloysite is almost unnoticed. If a clay is principally halloysite, 10 to 15 percent kaolinite could easily be overlooked, and electron microscopy techniques would be necessary for a positive identification.

The tubular form of halloysite eliminates almost entirely a preferred orientation in samples, thus the basal reflections (of the (00ℓ) type) are less intense and more diffuse than those encountered in kaolinite. The non-orientation of halloysite by simple sedimentation pointed toward a different morphology than that of kaolinite. This has been confirmed by Bates (6) and others by electron microscopy, where the existence of tubular crystals, as well as split and unrolled tubes, has been observed.

The basal spacing of the dehydrated form is about 7.2 Å, and of the hydrated form, 10.1 Å. The difference, 2.9 Å, is approximately the thickness of a sheet of single water molecules. On this basis, Hendricks (9) proposed a structure (Figure 4) which explains the (001) and (003) reflections and the absence of the (002) reflection, the easy dehydration

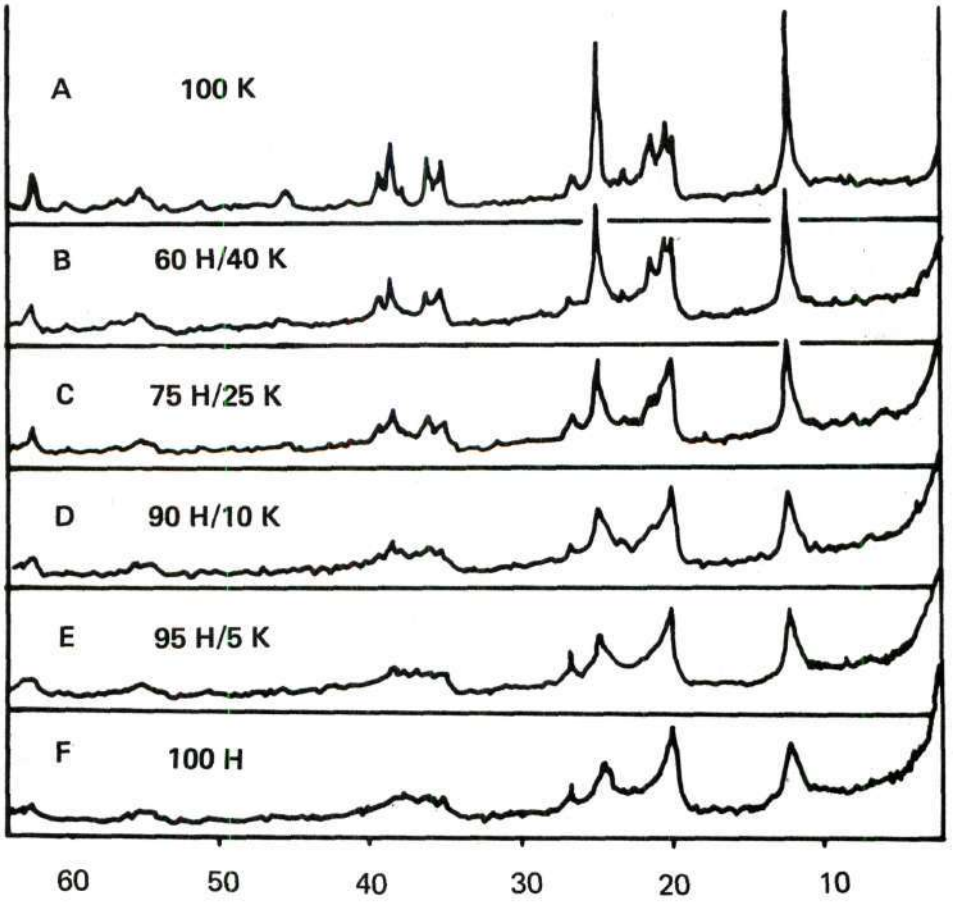

Figure 3. X-Ray Powder Diffraction Patterns of Prepared Mixtures of Kaolinite and Halloysite.

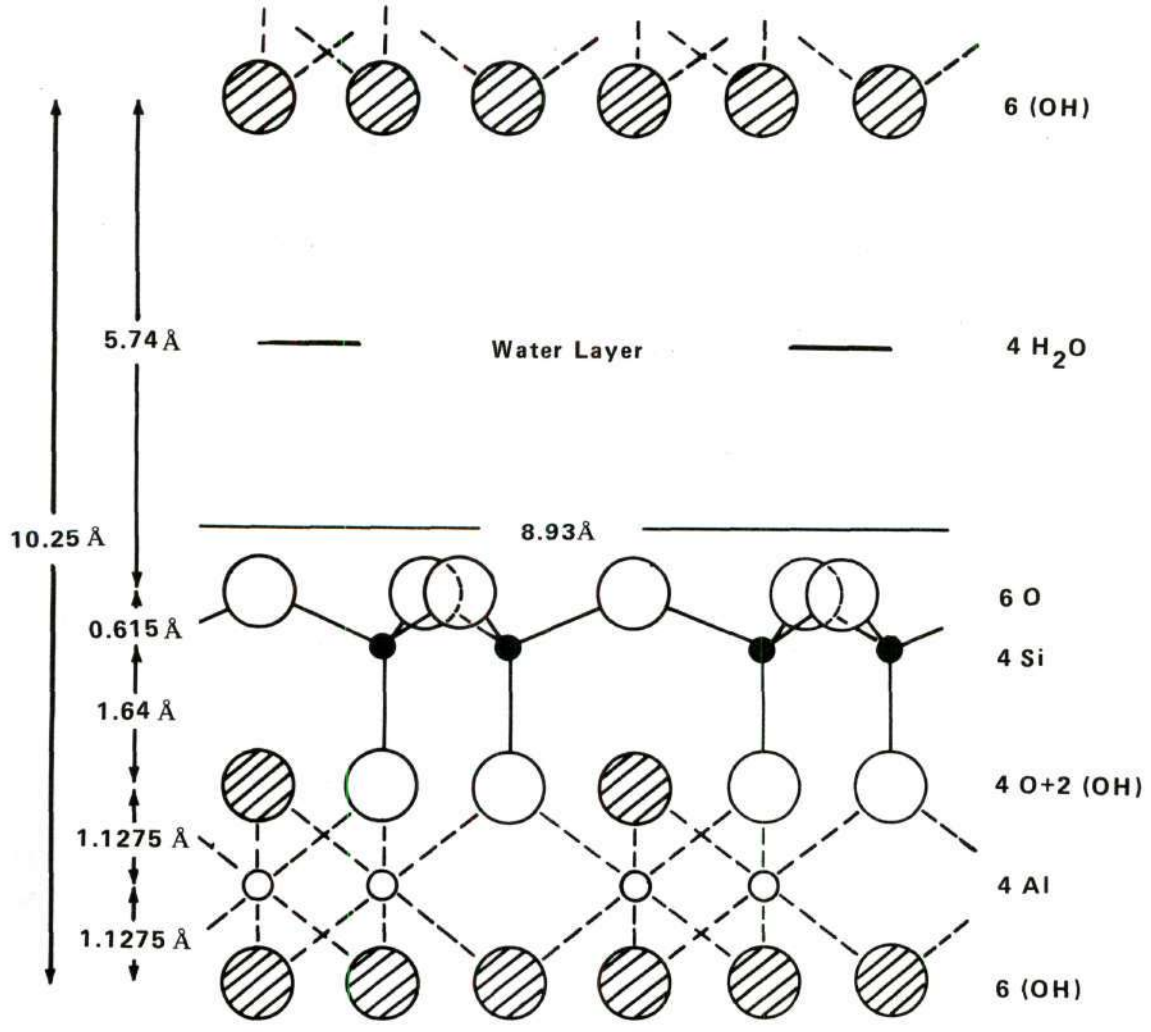

Figure 4. The Structure of Halloysite According to Hendricks.

without change of layer structure, and the additional 2 H_2O in the highly hydrated form.

Halloysites dried at 110°C have strong reflections for spacings at about 7.2 - 7.5 Å and 3.6 Å, corresponding to the (001) and (002) reflections from kaolinite. In addition, there are diffuse bands which can be indexed as (hk) two-dimensional diffraction peaks. The absence of sharp reflections can be attributed to an irregular stacking sequence.

Grim (10) postulates that halloysite consists of layers similar to those in kaolinite but randomly displaced parallel to both the a- and b-directions. The displacements are thought to be simple fractions of the cell dimensions. As in the other kaolin minerals, there is a 1:1 structure in which a modified gibbsite sheet (Al-OH) is bonded to a Si-O sheet. The height of the resulting unit in the c-direction is 4.51 Å. In gibbsite the six hydroxyl ions on one side of the unit cell occupy a distance of 8.62 Å, while in the Si-O sheet in kaolinite, the corresponding six oxygens occupy a distance of 8.93 Å. Thus, as Pauling (11) pointed out, the two planar sheets which make up the structure will not form a perfect fit.

The occurrence of tubular forms has been attributed to the strain resulting from the binding of the Si-O and Al-OH sheets together. According to Brindley (12), a minimum strain will exist in a layer which is curved so that the Si-O and Al-OH sheets have their own characteristic dimensions, b_o = 9.16 Å for the Si-O sheet and b_o = 8.75 Å for the Al-OH sheet. This corresponds to a diameter of about 150 Å. According to Bates (5), hydrated halloysite has a silicate sheet of diameter 150 Å as the innermost layer. Alternate layers of water and silicate may then be added,

although increasing the strain with each layer. At some maximum value, the strain will prevent any future growth.

Dehydration of Hydrated Halloysite

Upon dehydration, halloysite loses two water molecules irreversibly, causing a splitting of the tubular crystal; a metahalloysite forms which, according to Brindley (13), has the composition $Al_2(Si_2)_5)(OH)_4 \cdot x\ H_2O$, where x varies from $\frac{1}{4}$ to $\frac{1}{2}$, and a lattice spacing in the range of 7.2 - 7.5 Å. Figure 5 shows a schematic cross section of a tube of halloysite according to Bates and Brindley. Hydrated halloysite shows significant water loss when heated to temperatures below 100°C; dehydrated and partially dehydrated forms do not show a significant loss. The water lost below 100°C consists of pore water and water contained between basal planes (10). Most of the interlayer water can be lost at room temperature over moderate periods of time; however, not all interlayer water is lost, with about one layer of water per four silicate layers remaining. Heating up to 400°C completes the removal of interlayer water. Brindley and Goodyear (13) showed that the complete loss of interlayer water is not accompanied by reorganization of the silicate layers. The interlayer water lost at room temperature is lost by an irreversible reaction. Experiments have shown that certain organic molecules, e.g., glycol, can penetrate between layers of dehydrated halloysite, but only if some interlayer water is present. Apparently, once all the interlayer water is lost, the hydrated form cannot be obtained again.

Above the temperature for the dehydration reaction of OH lattice water, the differential thermal curves of some halloysites are very similar to those for well-crystallized kaolinite. This would suggest that

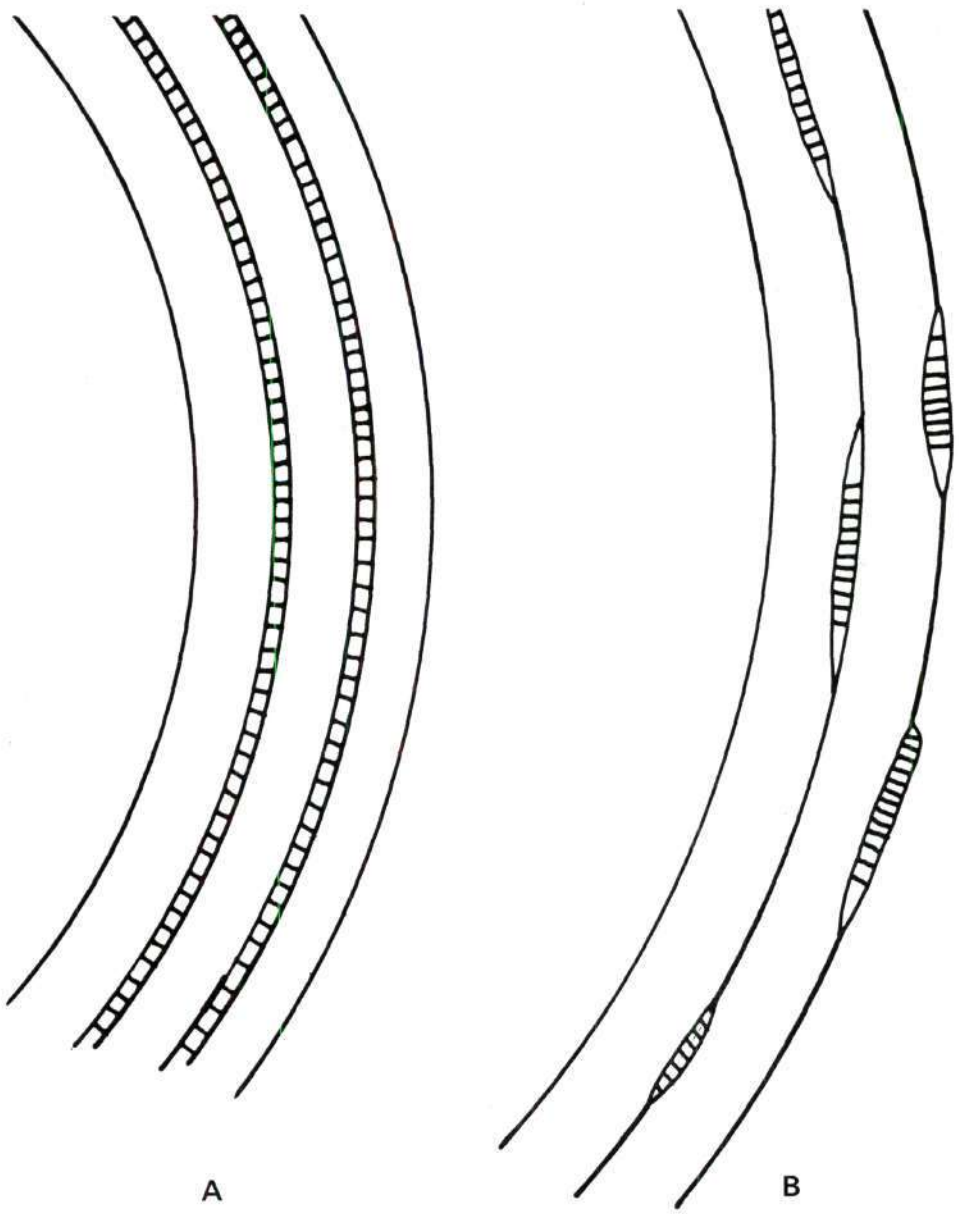

Figure 5. Cross Section of Halloysite Tubes.
(A) Bates' Suggestion for the Structure of Hydrated Halloysite.
(B) Brindley's Suggestion of Partially Dehydrated Halloysite.

some structure is retained after dehydroxylation. It is not known if this is characteristic of all halloysites (10). Grim and Bradley (14) showed that halloysite, after being heated to 600°C for one hour, regains only a very small amount of OH lattice water after 70 days at room temperature.

Attempts to reconstitute dehydrated halloysite by hydrothermal treatment have not generally been successful, and even in the most successful cases, there is much less change than for kaolinite.

Neutron Scattering

X-ray diffraction has been the principal method of crystalline structure analysis of kaolin and halloysite minerals up to the present time. In recent times neutron diffraction has been applied to many structures containing hydrogen, especially where hydrogen atom positions are of central importance. The motivation for using neutron diffraction in these cases can be understood in terms of the differences between x-ray and neutron scattering. X rays are scattered from the atomic electrons and the strength of this scattering is proportional to the atomic number. Thus, the scattering of x rays from hydrogen in a structure containing heavier atoms will not be readily seen. By contrast, neutrons are scattered (in a non-magnetic substance) by the nuclei of a material where no simple relationship between atomic number and scattering power exists (15). In particular, the neutron scattering strength of hydrogen is comparable in magnitude to most of the elements.

The neutron scattering properties are conveniently described in terms of cross sections, where cross sections can be regarded as the cross

sectional area presented by the nucleus to the incident neutron for a scattering process, including neutron capture (absorption). Thus, as the cross section increases, the probability for a scattering process increases. Since there is no sufficiently detailed knowledge of nuclear scattering processes, values of the cross sections must be determined by experiment. For most neutron scattering studies only three types of cross section are required. These are the coherent scattering cross section which is proportional to those scattering processes which give rise to atomic structure diffraction effects, the incoherent scattering cross section which is proportional to a nuclear disorder scattering that is independent of atomic structure, and finally the absorption cross section which is proportional to the neutron capture process. The scattering amplitude is related to the scattering cross section as the radius is to the area of a circle. That is, the cross sections for scattering are obtained by appropriate squares of scattering amplitudes.

The scattering amplitudes and their relation to atomic number are compared with the corresponding quantity for x-ray scattering in Figure 6. It can be seen that the x-ray scattering amplitude is proportional to Z, the atomic number.

Scattering amplitudes may be greatly affected by isotope effects and spin states. Deuterium, for example, has a positive scattering amplitude, while hydrogen has a large negative amplitude. The sign of the hydrogen amplitude is related to the proximity of the resonance absorption energy (analogous to x-ray dispersion corrections for wavelengths near the K edge). A neutron may combine with a target nuclei to form a "compound" nuclei. If the total energy is near a resonance level, scatter-

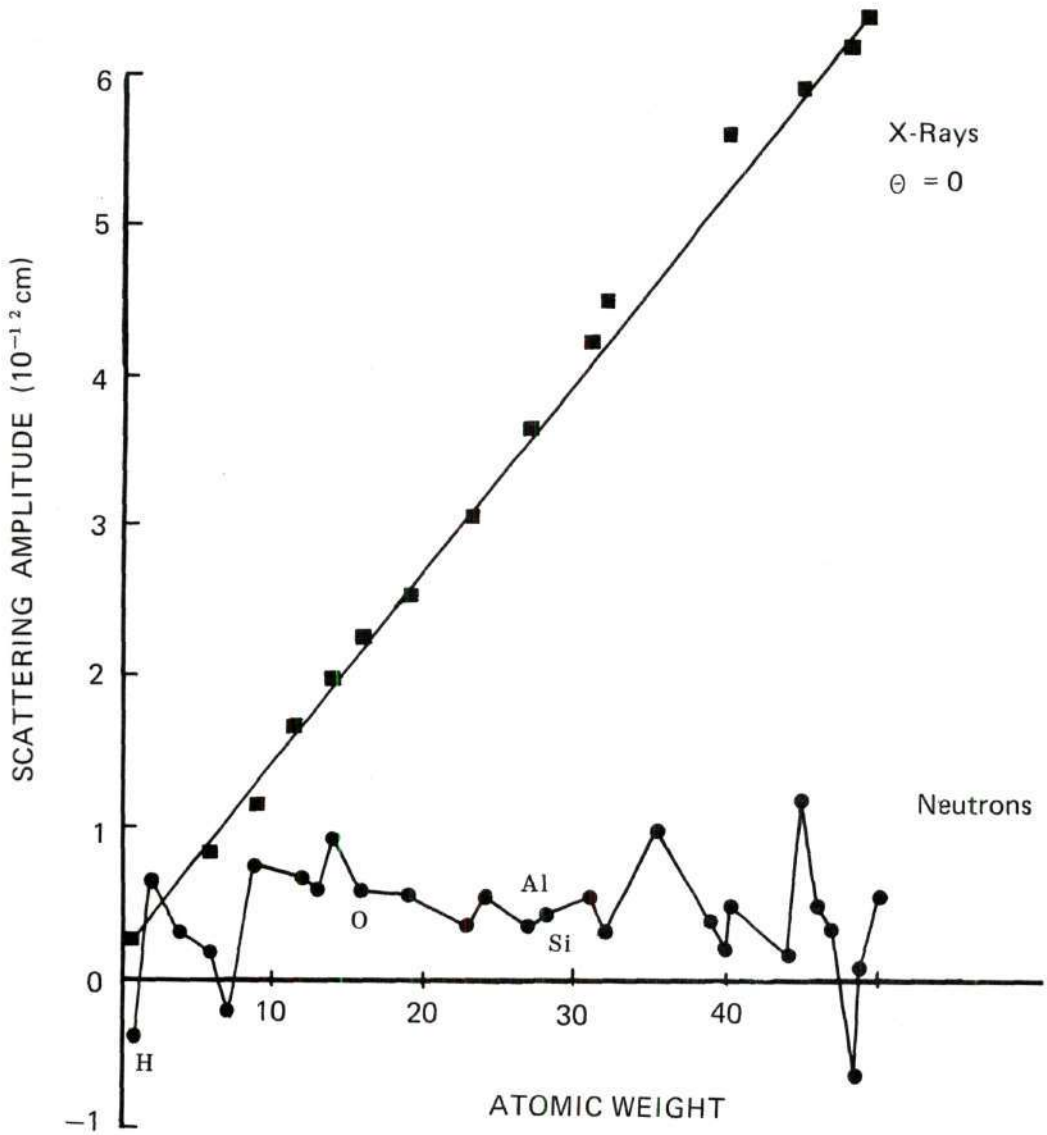

Figure 6. Variation of Scattering Amplitudes With Atomic Weight.

ing is produced. If the target nuclei has a spin, I, neutrons, with spin $\pm \frac{1}{2}$, may interact to modify the scattering. This is termed spin incoherence, of which the best example is hydrogen. Hydrogen nuclei have randomly oriented spins, which react with a neutron beam to produce incoherent scattering, which increases the diffuse background of a neutron diffraction pattern.

X-ray and neutron scattering patterns are similar in regard to Bragg reflections. Both show such effects as two-dimensional broadening caused by layered lattices. Both show the same (hkℓ) reflections in general, except that differing relative intensities amongst the reflections may be observed between the two patterns.

Experimentally, however, the practical aspects of procedure are quite different. The beam attenuation is small and is due primarily to scattering. Since most research reactors operate at relatively low flux levels, longer counting times and much larger samples are required to produce statistically satisfactory results.

There are several non-Bragg effects which are more significant in neutron scattering than in x-ray scattering. Thermal diffuse scattering increases with diffraction angle similarly to x rays, and can usually be neglected for relatively small angles. Incoherent scattering may produce very large backgrounds on neutron diffraction patterns, especially if hydrogen is present. Due to the large sample sizes required, a neutron may undergo several scattering events before leaving the sample. This multiple scattering results in a redistribution of scattered intensities and serves to further increase the diffuse background. Fortunately, the multiple scattering contribution to the diffuse background is a calculable quantity.

CHAPTER III

INSTRUMENTATION AND EQUIPMENT

Three techniques were selected for specimen characterization: impurity analysis, lattice parameter determination, and scanning electron microscopy. Impurity analyses were made with a Norelco Universal Vacuum X-Ray Spectrograph. The tungsten target x-ray tube was maintained at 50 kilovolts and 50 milliamperes. For the analysis of elements between atomic number Z = 13 to Z = 21, it was advantageous to use an ethylene diamine d-tartrate (EDDT) analyzing crystal and a gas-proportional counter. The EDDT crystal has a large d value and relatively low absorption for the softer radiation emitted by lower atomic number elements. For the analysis of elements with Z greater than 21, a lithium flouride crystal and a scintillation counter were used. Both crystals were oriented to diffract from a cleaved (200) face. The beam was collimated with Soller slits, with an entrance of 0.025 inch and exit of 0.040 inch. A powder sample of approximately one gram was maintained in the vacuum chamber of the spectrometer at 100 microns of mercury. A National Bureau of Standards clay was used as a reference standard.

Lattice parameter measurements were made with a standard Hull-Debye-Scherrer powder camera of diameter 114.6 millimeters. The Straumanis loading technique was used. Films were read on a Norelco film reader calibrated to an accuracy of 0.5 mm.

The morphology of halloysite was investigated with a Stereoscan

Mark II A Scanning Electron Microscope developed by Cambridge Instrument Company. A fine probe of electrons accelerated by a potential of 30 kilovolts was directed onto the specimen. A specimen image having excellent depth of focus can be observed by recording of the secondary beam which is a relative measure of the topography of the specimen. A short persistence high-resolution cathode ray tube was used to display the secondary beam for photographic recording.

Two thermal methods were used to follow the dehydration processes. Differential Thermal Analysis (DTA) was used to study endothermic and exothermic reactions as a function of temperature. A 25 mg sample was heated in a circular furnace in an air atmosphere, from room temperature to 1100°C, at a rate of 15°C per minute. Calcined alumina was used as a reference standard because it undergoes no thermal reactions in this temperature range. The process was controlled and recorded by an R. L. Stone Environmental Control System.

Thermal Gravimetric Analysis (TGA) was used to study weight loss as a function of temperature. A platinum bucket suspended from a thin platinum wire held a 13.25 mg sample. The sample and balance were contained in an evacuated Vycor vessel, and the sample heated by a platinum-wound furnace. The weight change was monitored on a Cahn RG electrobalance. The experiment was controlled and recorded by an R. L. Stone Environmental Control System.

Structural characterization and dehydration processes were monitored using x-ray and neutron diffraction. X-ray diffraction analyses were made with a Norelco diffractometer, using a copper target x-ray tube, a nickel filter, and settings of 40 kilovolts and 20 milliamperes. A

sealed proportional counter was used as a detector with a receiving slit of 0.003 inch, and a one degree aperture for the diverging beam. The pulse height analyzer was set at 90 percent, with a time constant of four.

Neutron diffraction analysis utilized a beam of thermal neutrons obtained from the Georgia Tech Research Reactor, operating at a power level of one megawatt. The neutron beam from the reactor was diffracted from the (200) plane of a large copper single crystal, giving a monochromated beam of wavelength 1.098 Å. Beam collimation consisted of two Soller channel collimators. A 45 minute divergence collimator was placed between the monochromator and specimen and a 39 minute divergence collimator was placed between the sample and the neutron detector. The detector was a BF_3 proportional counter of two inch diameter and a 12 inch active length. Step recording of scattering patterns was automatically controlled with timing determined by a low efficiency neutron detector in the incident beam. The schematic experimental configuration is shown in Figure 7.

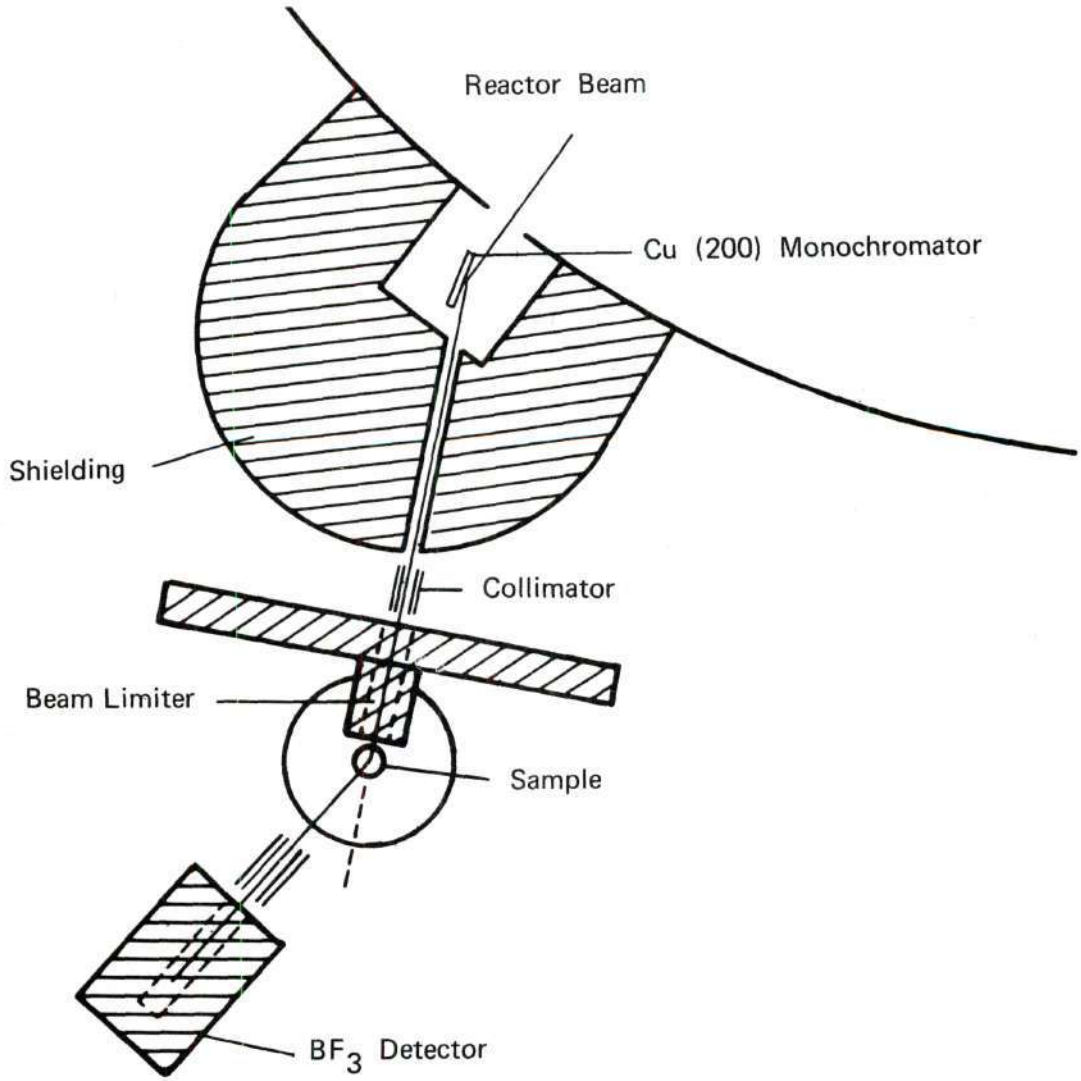

Figure 7. Experimental Configuration for Conventional Neutron Diffraction.

CHAPTER IV

EXPERIMENTAL PROCEDURE

Specimen Characterization

A well-crystallized hydrated halloysite sample from Chattooga County, Georgia was investigated. The sample was contaminated with small nodules of iron oxides (hematite) which could easily be removed, leaving a very white, pure specimen. After removing the contaminants and stained areas, the sample was pulverized in an electric mortar and stored in an air-tight vessel at 10°C.

X-ray fluorescence spectroscopy was used to determine the impurities present in hydrated halloysite. An initial scan indicated the impurity elements chromium, calcium, iron, titanium, potassium, and zirconium. A 2θ value satisfying the Bragg condition for $K\alpha$ emission was set for each element. Intensity measurements were made by recording and summing counts per second for each peak. Intensities of impurity element peaks were compared to intensities of a National Bureau of Standards clay for quantitative measurement. The pulse height analyzer was set at 80 percent for the iron determination in order to keep the fluorescence signal on a convenient scale. A setting of 90 percent was used for all other elements. The calculated percentages of impurity elements are given in Table 1.

Table 1. Impurity Analysis of Hydrated Halloysite

Impurities	Atomic Percentages
Calcium	0.0031
Chromium	0.0063
Iron	0.8445
Potassium	0.0543
Titanium	0.0323
Zirconium	0.0026

The crystallite size was esimtated from x-ray diffraction peak widths. A strain-free Norelco silicon wafer of crystallite size greater than 1000 Å was used as a standard. A diffraction pattern was recorded over the angular range 2-90° at $\frac{1}{8}$° 2θ per minute. The instrumental peak breadth, b, was obtained by measuring the peak width at one-half height using CuKα reflections.

A powder sample of hydrated halloysite was scanned in the same manner, and the width at half height, B_o, of (00ℓ) peaks was measured. The $K\alpha_1$ and $K\alpha_2$ reflections were unresolved, however, and the width was corrected for doublet separation. The peak widths of hydrated halloysite were then corrected for instrumental broadening, and by assuming a near-Gaussian peak profile, the broadening due to crystallite size, β, was computed graphically. The mean crystallite size, D, was calculated by the Scherrer equation:

$$D = \frac{K\lambda}{\beta \cos\theta} \qquad (1)$$

The (00ℓ) reflections were the only distinct peaks suitable for crystallite size determination. The remaining (hk) reflections trailed off

so slowly on the high-angle side that an accurate peak width determination was impossible.

An attempt was made to determine the contribution of strain in the sample on the peak broadening. Procedures for strain determinations are applied more readily to studies of metals, but it was hoped that a difference in strain before and after dehydration could be detected. With only two reflections suitable for use as data points the results cannot be quantitatively meaningful, but it was concluded that strain was too small to be observed and did not contribute to peak broadening.

The mean crystallite size for hydrated halloysite was 193 Å. After heating to 100°C for one-half hour, the value was 180 Å. A sample calculation is shown in Appendix A.

The relative rates and temperatures of thermal reactions were determined by differential thermal analysis (DTA). Small thermocouples monitor the difference in temperature between the sample and the thermally inert standard. The differential signal is plotted against temperature as the two samples are heated at a constant rate of 15°C per minute. Evidence of thermal reactions was recorded as either positive (exothermic) or negative (endothermic) deviations from a central base line on a strip chart recorder.

Weight loss as a function of temperature was determined by thermal gravimetric analysis (TGA). A small thermocouple positioned at the same level as the sample monitored the temperature, which was programmed to increase at a rate of 15°C per minute. To check for non-linearity in the heating rate, a calibration curve was obtained under identical experimental conditions using an empty sample container.

The weight loss was continuously monitored as temperature increased. The loss was recorded on a strip chart, with a maximum deflection corresponding to a 0.02 g loss of weight. Samples of hydrated halloysite were heated to approximately 300°C. Several specimens were heated to lower temperatures in order to check the accuracy of the data.

Investigation of the Dehydration Process

X-Ray Diffraction

X-ray diffraction analysis was used to study structural changes in hydrated halloysite with increasing temperature. The specimens were heated at a rate of approximately 5.5°C per minute in an electric muffle furnace. Samples were held for one hour at 50, 100, 150, 200, and 300°C, cooled in a dessicator and analyzed by x-ray diffraction. Diagrammatic diffraction patterns are given in Figure 12.

Several slides were coated with a water slurry of the powder specimens and allowed to air dry. Diffractometer traces were similar to those obtained for powder samples, indicating that there were no obvious preferred orientation effects.

Several powder specimens were heated to 450°C for one hour and x-rayed. After periods of up to three months in water, samples were again x-rayed to determine if any rehydration had occurred.

Neutron Diffraction

Diffraction patterns were obtained over the angular range 4° - 26° 2θ with a wavelength of 1.098 Å. Samples were heated to 50, 100, 150, 200, and 300°C. This range contained three major reflections, the (001), (02), and (002), which are most affected by dehydration and afford an oppor-

tunity to observe both two- and three-dimensional diffraction effects. For cylindrical specimens completely bathed in the neutron beam, the integrated intensities of the Bragg diffraction peaks in neutron counts are given by:

$$\text{counts} = \left(\frac{\lambda^3}{8\pi}\frac{\ell}{R}\right) M \cdot \frac{j N_c^2 F_{hk\ell}^2}{\sin\theta \sin 2\theta} A_{hk\ell} \qquad (2)$$

where

λ = wavelength of neutron beam

ℓ = height of counter slit

R = distance from counter to specimen

M = mass of specimen in beam

j = multiplicity

N_c = number of scattering nuclei per unit cell

$F_{hk\ell}$ = structure amplitude factor

$A_{hk\ell}$ = absorption factor

Parameters in the parentheses remain constant for the diffraction geometry used in these experiments.

The incoherent scattering contribution is similarly related to an instrumental constant, the number of nuclei in the specimen and the scattering cross section. The neutron counts per unit time is written:

$$\text{Counts/time} = K\left[\sum_i N_i \sigma_i/4\pi + P_{ms}\right] A + B \qquad (3)$$

where the summation is made over all the nuclei in the specimen, N_i is the number of each type of nuclei, $\sigma_i/4\pi$ is the incoherent scattering cross section per steradian, K is the instrumental constant, P_{ms} is the

multiple scattering contribution, A is the absorption factor, and B is an instrumental background counting rate.

The instrumental constant can be determined with the use of a standardization experiment in which a known scatterer is used as the specimen. In detail, the procedure requires the determination of the sample mass, neutron transmission and cylinder specimen geometry. A background scattering correction is simply determined from a scattering pattern without the specimen. From these data, the number of nuclei can be calculated, the multiple scattering correction can be assessed, and the appropriate absorption correction can be taken from tables. These procedures are below. And then the application of these procedures to the determination of hydrogen content is summarized.

Transmission of Neutron Beam. Measurements of the transmission of the neutron beam were made with a 4 mm beam passing through the center of the sample. The beam was defined by a boron carbide block with a stainless steel tube having a 4 mm inside diameter passing through the block. The neutron detector was set at 0° scattering angle. Since one is interested only in the thermal neutrons, the fast neutrons (< 5 percent) were eliminated by subtracting the neutron counts which were recorded when a 0.46 mm cadmium sheet was placed in the beam. (Cadmium blocks out thermal neutrons while essentially passing the fast neutrons.) The relative transmission is given by the expression

$$T = \frac{I_T - I_T^{Cd}}{I_o - I_o^{Cd}} \tag{4}$$

where I_T is the transmitted intensity, I_o is the incident intensity, and

Cd superscript refers to the cadmium transmission intensities. This transmission ratio is related to the attenuation factor, μ, and the sample cylinder diameter, D, by the relation

$$T = e^{-\mu D} \tag{5}$$

The exponent, μD, is then used to calculate the attenuation factor, A, in equation (3). The data and calculations for each of the specimens are given in Appendix C.

Multiple Scattering Contribution. The extra scattering contribution due to multiple scattering is a function of both the specimen geometry and scattering properties and must be calculated by a relatively involved integration procedure. Fortunately, the multiple scattering effects for a cylindrical sample of radius, R, and height, h, have been calculated by Blech and Averbach (16). The ratio of multiple scattering to total scattering is given in the formula

$$\frac{\sigma_{ms}}{\sigma_s} = \frac{\delta(\sigma_s/\sigma_T)}{1-\delta(\sigma_s/\sigma_T)} \tag{6}$$

where σ_{ms} is the multiple scattering cross section, σ_s is the total scattering (coherent and incoherent) cross section, σ_T is the total scattering plus absorption cross section, and δ is the multiple scattering parameter which has been tabulated by Blech and Averbach as a function of (the transmission exponent of equation (5) divided by 2) and R/h. A simplification applies to the scattering from a hydrogenous scatterer, since, as shown in Table 2, the ratio σ_s/σ_T is approximately unity. Thus,

$$\frac{\sigma_m}{\sigma_s} = \frac{\delta}{1-\delta} \tag{7}$$

After experimentation with several geometries, it was concluded that a specimen of small radius would be most advantageous in reducing multiple scattering contributions. Thus, an aluminum tube of $\frac{1}{4}$ inch was employed in these experiments. The calculation of multiple scattering contributions as a fraction of the observed diffuse scattering is tabulated in Appendix C.

Table 2. Neutron Cross Sections for Atoms in Halloysite

Atom	σ_{coh} (barns)	σ_{inc} (barns)	σ_a (barns)
Al	1.5	0	0.13
H	1.79	79.71	0.19
O	4.2	0.02	0.0001
Si	2.16	0.04	0.06

Determination of Absolute Hydrogen Content. Approximately one gram of hydrated halloysite was used in the one-fourth inch diameter aluminum sample holder. Diffraction patterns over the angular range 4° - 26° 2θ were recorded for samples heated to 50, 100, 150, and 200°C. Fixed time counting of two minutes per point was used for increments of 0.2° 2θ. To minimize water absorption, the samples were heated immediately before use and sealed in the sample container. The recorded intensities were first corrected for background, then the multiple scattering contribution was subtracted. The intensities were again adjusted so that the counts were

proportional to the number of grams of sample in the beam.

V_2O_5 was used as a standard scatterer because of its high purity and because the incoherent scattering cross section of vanadium is well known. In addition, the sample, in a $\frac{3}{4}$ inch diameter aluminum holder, gives rise to small multiple scattering contributions.

Once K is determined for the particular geometry using equation (3), K can be used in a similar equation to solve for the number of nuclei of halloysite.

From Table 2 it can be seen that the cross section for incoherent scattering by hydrogen is overwhelmingly large, and, therefore, the remaining background on the corrected diffraction patterns was attributed entirely to hydrogen incoherent scattering.

CHAPTER V

DISCUSSION OF RESULTS

Preliminary experimentation was conducted to characterize the hydrated halloysite specimen's purity, morphology, degree of crystallinity, and thermal behavior. These experiments were primarily to study qualitative aspects and will be discussed on this basis. After characterization of the sample, the dehydration process will be considered. X-ray and neutron diffraction were used to study structural changes that occur during dehydration. X-ray diffraction shows most clearly the changes involved when water is lost from hydrated halloysite, i.e., the shift in the basal reflections. Neutron diffraction confirms this observed decrease in the lattice dimensions, but has the further advantage that it also offers a means to calculate the loss of hydrogen quantitatively. Finally, the loss of hydrogen as determined by thermal analyses and neutron diffraction will be correlated and the differences and similarities discussed as to physical significance in the dehydration process.

Specimen Characterization

X-ray fluorescence was used to determine the impurity elements present in hydrated halloysite. The total impurities comprised 0.94 percent of the sample, which is quite low and compares favorably with halloysite standards of the American Society for Testing and Materials (A.S.T.M.) and the American Petroleum Institute.

The scanning electron micrographs confirmed the tubular morphology of hydrated halloysite as shown in Figures 8 and 9. The fact that some of the tubes are split is due to loss of water, which helps to bind the layers together. Some dehydration obviously occurs during specimen preparation.

Differential thermal analyses were performed to determine the temperatures of dehydration, and as an indication of the amount of water lost, the area under the first endothermic peak being proportional to the energy required to facilitate the dehydration process. Loss of water is essentially complete when temperatures of about 400°C are reached. Above this temperature, in the range of 400-430°C, dehydroxylation begins, terminating at about 520°C; for higher temperatures, the DTA curve is essentially the same as that of kaolinite.

Halloysite and hydrated halloysite give only one major endothermic peak below the dehydroxylation temperature. From Figure 10 it is seen that this occurs between 50-100°C. However, this must be interpreted with a knowledge of the rate of heating. The thermal curves of Figure 10 were obtained by heating at 15°C per minute. Slower heating rates would broaden the peaks. X-ray diffraction patterns of hydrated halloysite heated to 50°C and below for one-half hour show that this major water loss can occur at temperatures below 50°C after a moderate time. Indeed, hydrated halloysite was found to lose water at room temperature if left in moderately dry air for several days. Figure 10 also shows very dramatically the substantial loss of water as hydrated halloysite loses water to form halloysite. DTA curves served merely as an aid in predicting and substantiating other experimental data, and no attempt was made to

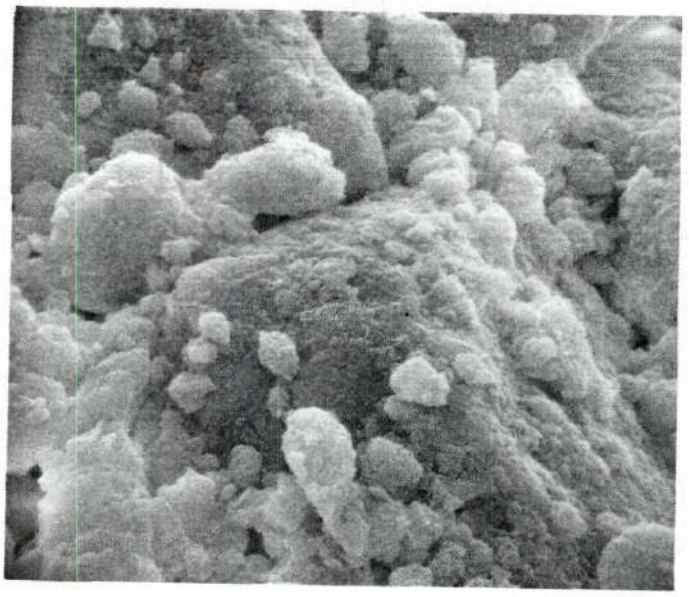

2000x

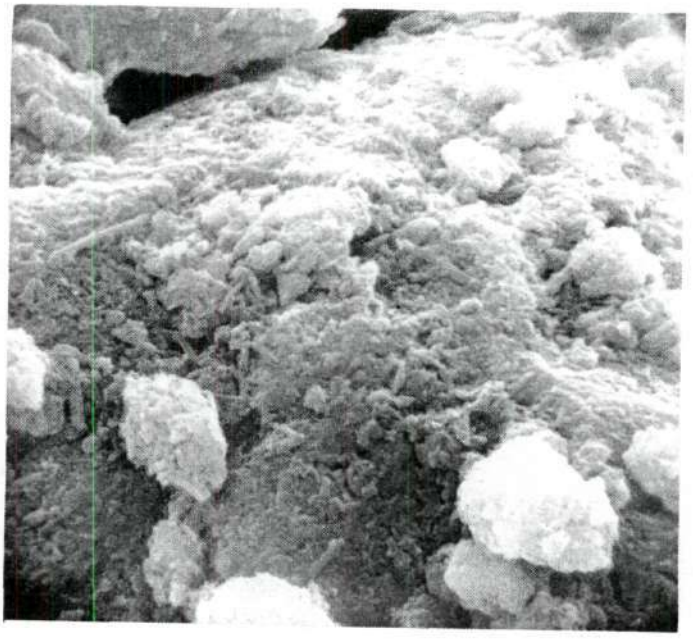

5000x

Figure 8. Scanning Electron Micrograph of Hydrated Halloysite.

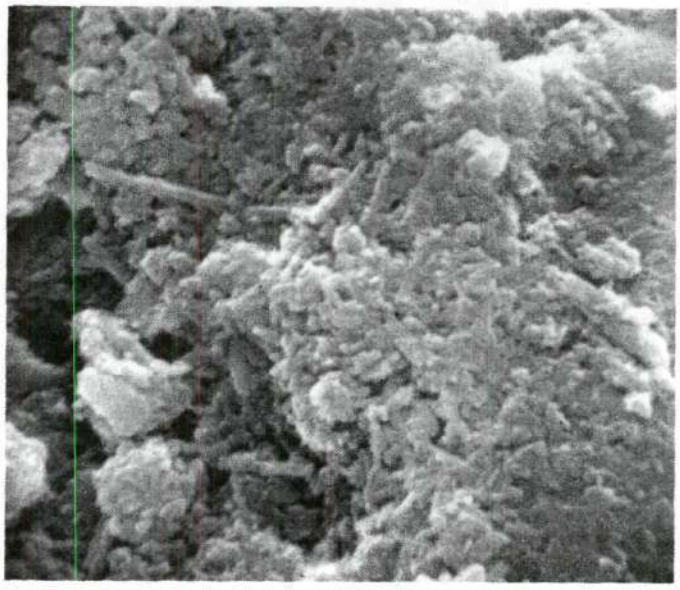

9200x

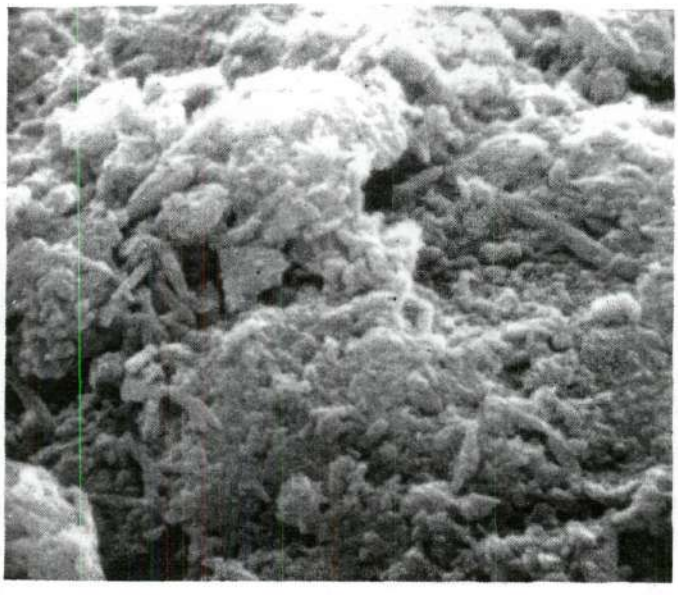

10,000x

Figure 9. Scanning Electron Micrograph of Hydrated Halloysite.

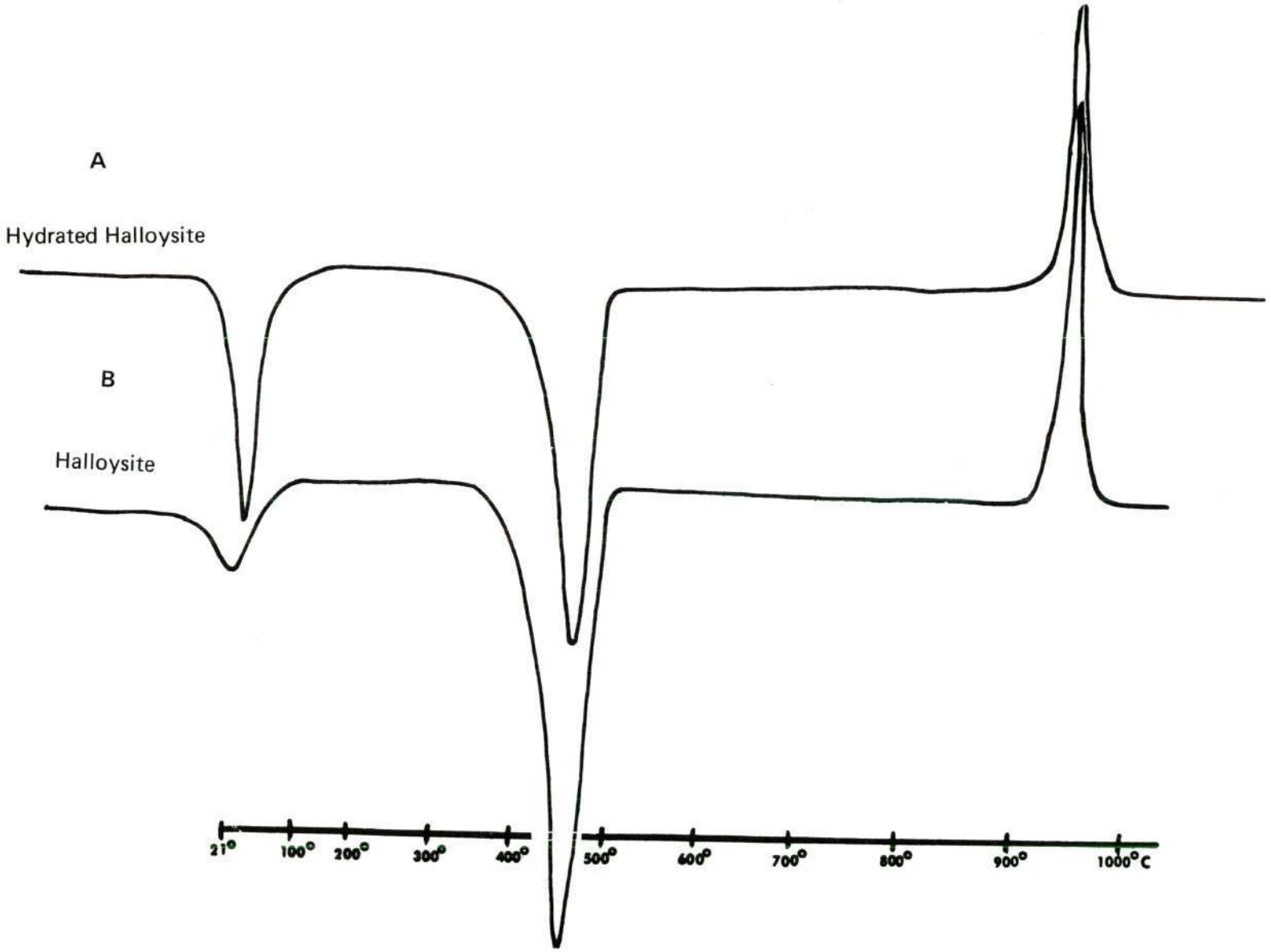

Figure 10. Differential Thermal Analysis Curves.
(A) Hydrated Halloysite
(B) Halloysite.

quantitatively interpret them.

Thermal gravimetric analyses (TGA) were used to study relative rates of weight loss with increasing temperature. The weight loss was considered entirely due to loss of water. The percent loss was calculated on the basis of the original sample weight. The weight loss as a function of temperature is shown in Figure 11. Hydrated halloysite is seen to lose water rapidly up to 100°C. This is consistent with the fact that partial dehydration will occur on heating to low temperatures for longer times or upon leaving the specimen in dry air. The initial water loss consists of absorbed surface water and interlayer water. The low temperatures required for removal indicate that the interlayer water is weakly bound. At higher temperatures the removal of interlayer water is completed, though it is not lost as easily.

X-Ray Diffraction Analysis of Dehydration

Hydrated halloysite gives a sharp basal (001) reflection corresponding to an interplanar spacing of 10.1 Å. Upon heating to 50°C for one hour, a diffuse, lower intensity peak forms corresponding to a 7.5 Å spacing, while the 10.1 Å peak loses intensity drastically, almost disappearing. Upon further heating to 100°C, the peak corresponding to the 7.5 Å spacing becomes sharper and more intense; in fact, heating for one-half hour or more at 100°C produces a pattern identical to halloysite (2 H_2O). Schematic x-ray diffraction patterns are shown in Figure 12.

Hydrated halloysite is generally considered to be built up of kaolinite unit cells, a Si-O tetrahedral sheet and an Al-OH octahedral sheet, joined together by layers of water. Considering this to be the case, the

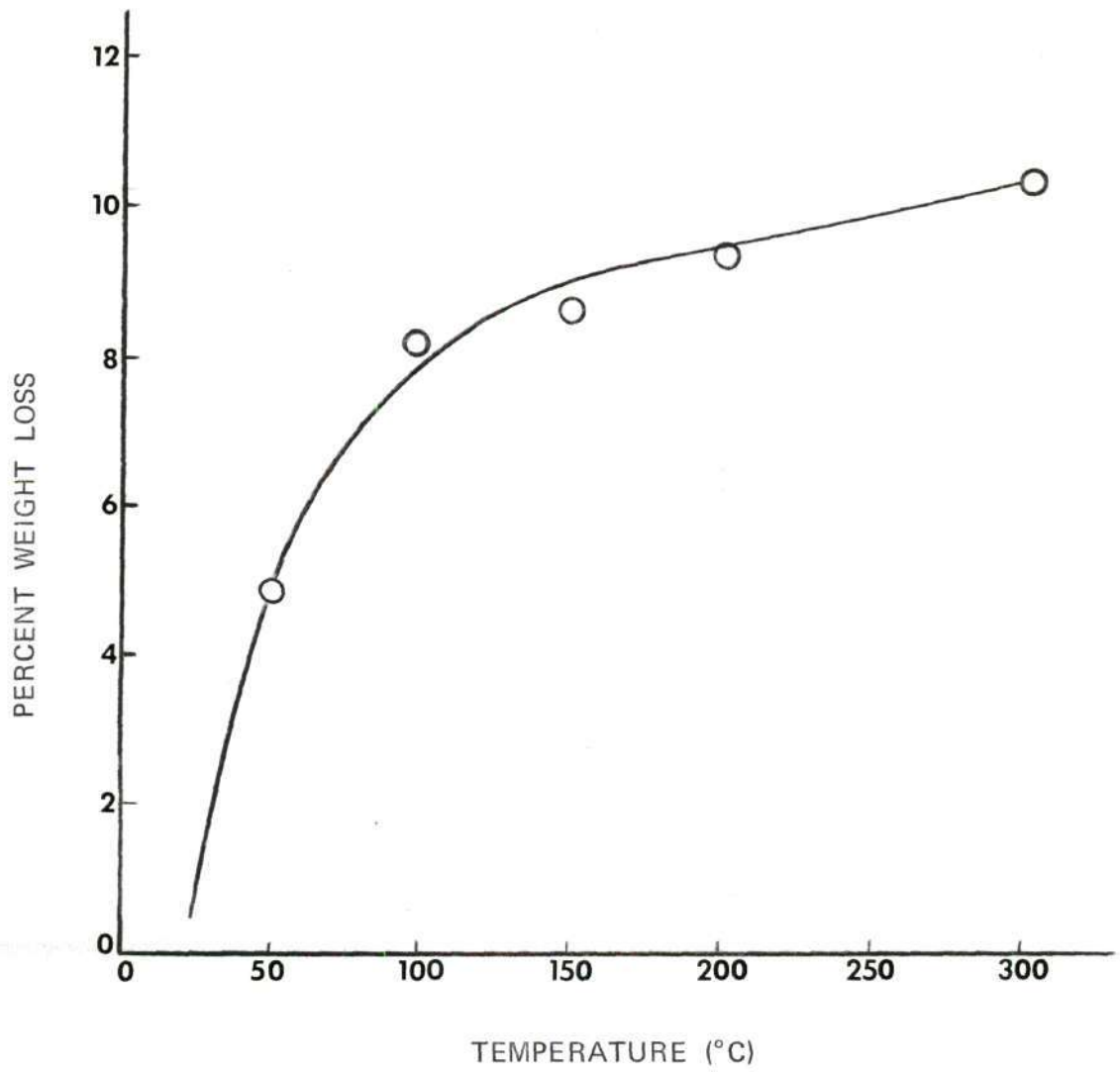

Figure 11. TGA Weight Loss as a Function of Temperature for Hydrated Halloysite.

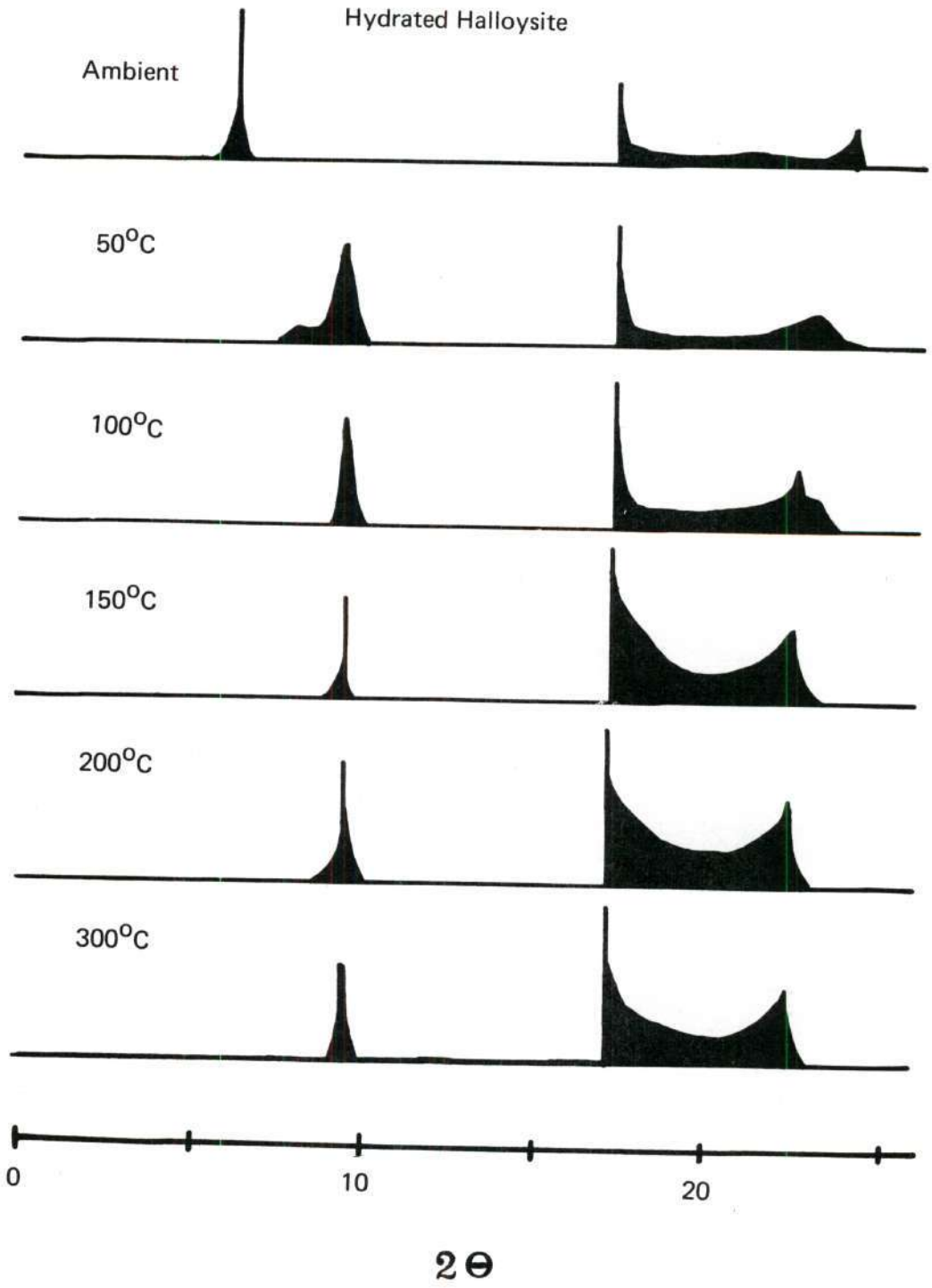

Figure 12. Schematic X-Ray Diffraction Patterns of Hydrated Halloysite.

water loss is observed in the shift of basal reflection corresponding to an interplanar decrease of 2.7 Å, which should correspond approximately to the thickness of the water layer.

If hydrated halloysite is ideally composed of kaolinite layers interleaved by water, then it is logical to assume that, upon dehydration, kaolinite will be formed. The fact that halloysite is formed, and not kaolinite, indicates two possibilities concerning the structure. First, if hydrated halloysite is composed of kaolinite unit cells plus water, the morphology of the two must be different. As first suggested by Pauling, the tetrahedral and octahedral sheets do not form a perfect fit, the difference in the dimensions being approximately 0.36 Å. Therefore, the most logical morphology in which the unit layers could assume their characteristic dimensions is a curved sheet. The water between consecutive unit cells probably serves to strengthen the bonding, actually making it possible for a tubular crystal to form and be relatively stable.

When the interlayer water is lost, the strain is increased, causing the tubular crystals to split and the (001) basal reflection to drop from 10.1 to 7.4 Å; the corresponding reflection for kaolinite is 7.2 Å. Also, in halloysite, the 7.4 Å (001) peak is smaller than the (02) band at 4.42 Å, which is the reverse of the kaolinite reflection intensities. This leads to the second possibility concerning the structure, the dehydration of hydrated halloysite is not accompanied by a rearrangement of the silicate layers.

The (001) reflection of hydrated halloysite is the one most drastically affected by heat. The (02) band remains unchanged, and the (003) reflection at 3.36 Å becomes obscured while a reflection at 3.63 Å (002)

emerges. It can therefore be concluded that the periodicity changes primarily along the c-axis, with little change in the a- or b-direction. Since the drop from 10.1 Å to 7.5 Å occurs so readily, it must be caused by loss of water, for no other reaction could proceed with such a small energy increase as heating to 50°C. Therefore, the (001) reflection in hydrated halloysite is a direct indication of the amount of water present. Unfortunately, x rays cannot scatter sufficiently from hydrogen for the atoms to be located, and all that is observed is the decrease in the basal parameters. With the (02) band as the most intense reflection, a structure composed of tubes of curved sheets located concentrically about the b-axis would indeed produce the observed x-ray pattern. For such a structure, the c-axis would be perpendicular to the axis of the tube.

Correlation of Dehydration Results

Hydrated halloysite was heated to different temperatures up to 300°C and investigated by x-ray and neutron diffraction. The x-ray diffraction patterns showed a gradual but drastic change in the (001) and (003) reflections. On heating to 50°C, the (001) reflection drops from 10.1 Å to a diffuse 7.5 Å peak. The (003) reflection weakens and the (002) reflection begins to appear. Further heating intensifies the new peaks, and there is little other change. These shifts indicate a change in structure, but not a destruction of the structure.

The neutron diffraction patterns, however, are quite different. The peak shifts are also very apparent, but most significant is a decrease in the diffuse background that underlies the Bragg reflections, as shown in Figure 13. The decrease in background is due almost entirely to the

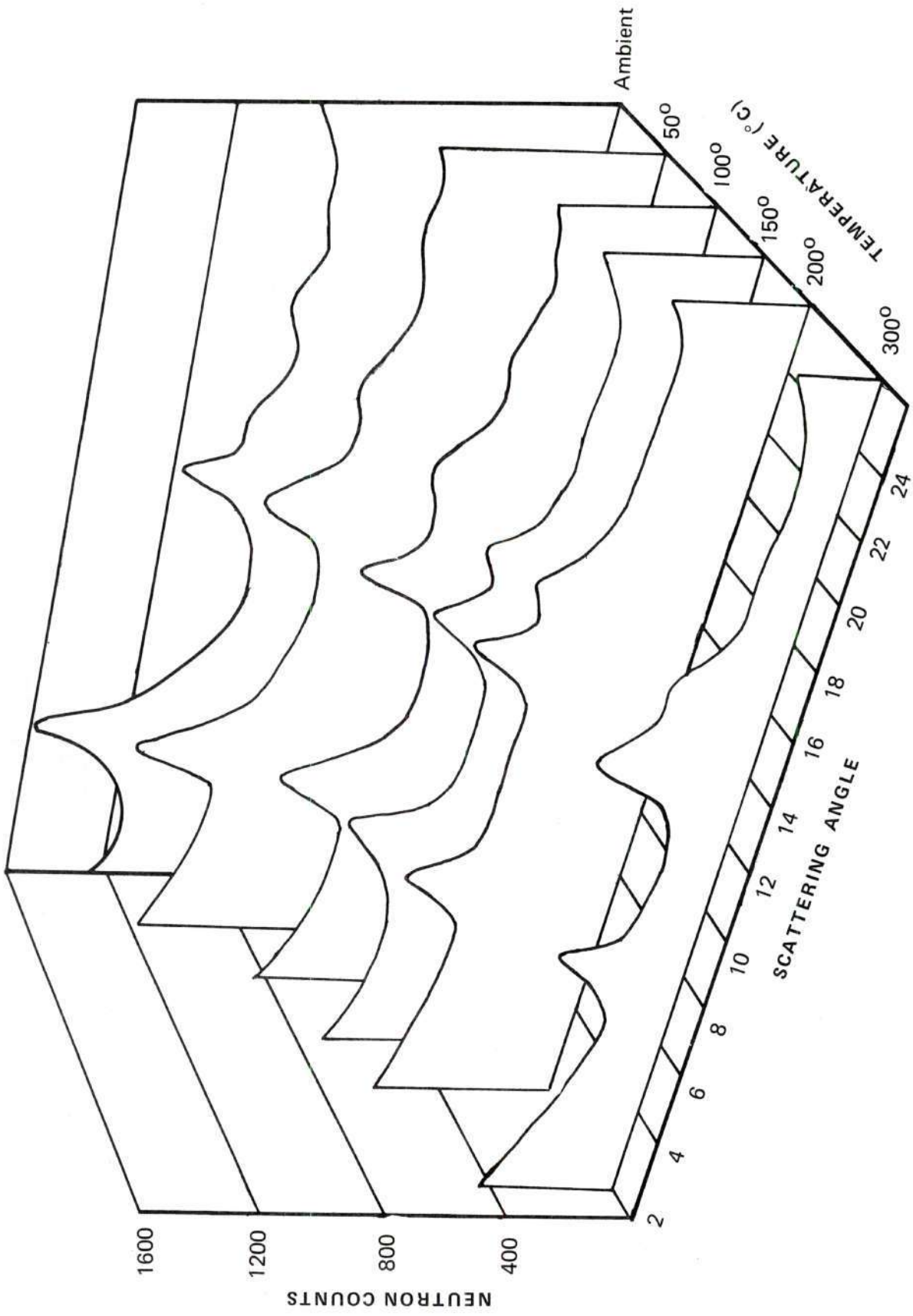

Figure 13. Neutron Diffraction Patterns of Hydrated Halloysite After Heating.

loss of hydrogen, which scatters incoherently and with an amplitude (negative) far greater than any other element in halloysite (Table 2). X-ray diffraction, therefore, can show structural changes but cannot be used independently to categorize these changes. On the other hand, neutron diffraction reflects completely what is happening, i.e., water is being lost.

The hydrogen loss, as calculated from neutron diffraction patterns, was converted to percent weight loss of water for comparison to TGA data on the assumption that no dehydroxylation occurs. This comparison, Figure 14, shows favorable correlation from ambient temperature to about 200°C, the difference being relatively constant and generally less than one percent. However, at 300°C, the neutron diffraction data give a weight loss of 12.5 percent, which is 2.4 percent higher than TGA weight loss. In the case of instantaneous weight losses which are only a function of temperature, the weight loss obtained by both methods should coincide, and the curve of Figure 14 should be a 45° line, as shown. The line is displaced one percent on the ordinate axis to account for absorbed surface water on the TGA specimen. TGA data are based on the weight of the original sample, thus surface water is necessarily included in the calculations. Hydrated halloysite, unfortunately, cannot be dried prior to testing because of the ease of dehydration and structural changes. The neutron diffraction specimen can be considered free of surface water due to sample preparation procedures.

The weight loss calculated from neutron diffraction, after an initial background correction, is based on an ideal specimen of hydrated halloysite, containing 4 H_2O. The weight loss calculation is based on an experimentally derived constant. Some discrepancy between the two data

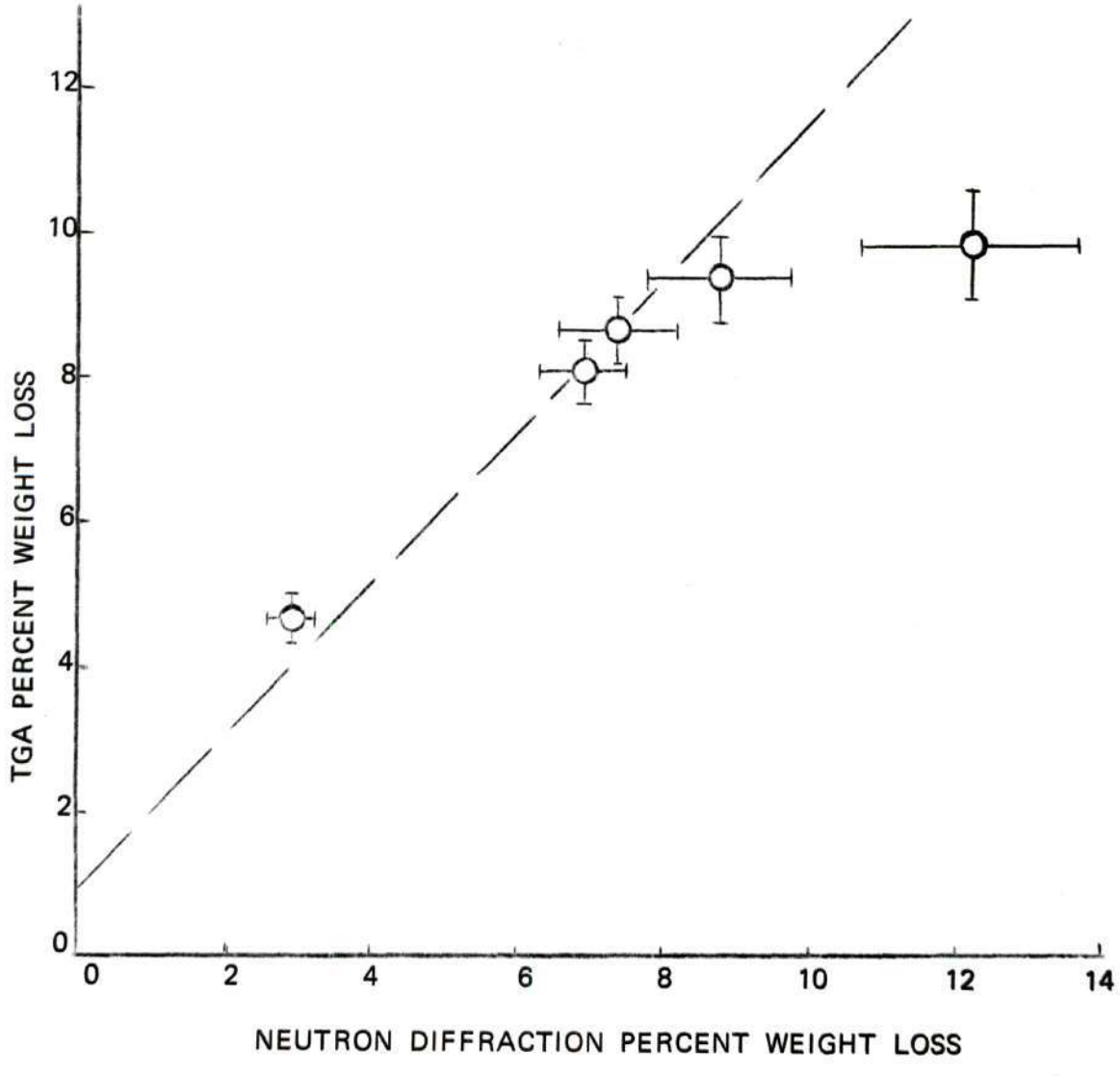

Figure 14. Correlation of Weight Loss Data.

sets might be anticipated, due to systematic errors arising from the use of the calibration constant and other associated corrections. The estimation of experimental error is shown in Figure 14 by statistical error bars, and ranges from 8 to 12 percent. The statistical neutron counting error increases with heat treatment temperature due to decreased neutron scattering intensities. The multiple scattering, along with associated errors, decreases slightly with temperature since hydrogen is lost and the incoherent scattering decreases. The background error is due only to counting statistics and is constant for all temperatures. TGA weight loss was assigned a maximum instrumental error of three percent.

The TGA weight loss must be considered as an "instantaneous" weight loss, for the sample is heated at a constant rate. Neutron diffraction specimens were heated for one hour at the specified temperatures, and it is expected that a larger weight loss would be associated with the extra length of heat treatment.

From Figure 11, it is seen that there is a rapid loss of water at low temperatures up to 100°C. Neutron diffraction data confirm this by showing a peak shift to a lower d-spacing and a drop in the diffuse background. The ease with which this occurs is conclusive that the weight loss is due entirely to interlayer and surface water. From 100 to 200°C, the weight loss is less drastic, indicating a removal of remaining water between unit layers. At 300°C, the higher value of the neutron diffraction data indicates that, with time, more water is lost. This may indicate the possibility that some structural hydroxyl ions may be lost at about 300°C if this temperature is held for some time.

It is believed that this is the first attempt to determine absolute

hydrogen content of a clay mineral. Calculations of this type, in which the actual number of protons can be found, may be very beneficial in investigating and differentiating other silicate minerals, from the montmorillonites and other complex clays to zeolites, in which absorbed materials play a very important role.

CHAPTER VI

CONCLUSIONS

1. The diffuse background underlying the Bragg neutron diffraction pattern can be used as a quantitative measure of the hydrogen present in the halloysite structure.

2. Hydrated halloysite forms in a tubular morphology which may be split upon loss of interlayer water.

3. The complete dehydration of hydrated halloysite is irreversible; partially dehydrated forms may be rehydrated in a moist environment.

4. Neutron diffraction water loss may be correlated with thermal data and may indicate thermal reactions not seen by standard thermal gravimetric analysis.

5. Neutron diffraction weight loss data deviations increase with temperature, suggesting that loss of bound structural water in halloysite may occur at lower temperatures than previously reported.

6. Neutron diffraction can be used to distinguish halloysite from kaolinite. Quantitative analysis of mixed clay minerals should, therefore, be possible.

7. X-ray and neutron Bragg diffraction patterns are essentially similar in the angular range investigated, suggesting that there are no unusual hydrogen ordered structures.

CHAPTER VII

RECOMMENDATIONS

There are several procedures involved in neutron scattering experiments that may ultimately determine the usefulness of the results. Such sources of error as multiple scattering or insufficient counting time may seriously affect results unless careful preliminary tests are used to eliminate these errors as much as possible.

Neutron diffraction has proven to be an exciting new method to further advance the studies of clay minerals and the strongest recommendation is that investigations of this type be continued. Neutron incoherent scattering thus far is the only means whereby detailed studies involving hydrogen are possible. Studies in the areas of hydrogen positions, dehydroxylation, dehydration, and absorption are badly needed to complete the characterization of clay minerals.

It is suggested that dehydration kinetics be investigated in halloysite and other clays. Quantitative energy calculations would be of great value in evaluating hydrogen loss in terms of bond strengths and orientations, and types of bonding. An experiment with great potential in many areas would be high temperature neutron diffraction, with a furnace mounted on the diffractometer. Information obtained in this way would be more readily comparable to other techniques and would no doubt be helpful in solving the many problems associated with clay research.

Quantitative analysis of clay mineral mixtures by neutron diffraction appears to be possible. Neutron diffraction studies should contribute as much to clay technology in the future as x-ray diffraction has in the past.

APPENDIX A

CRYSTALLITE SIZE DETERMINATION

Crystallite size determinations were made by methods outlined by Klug and Alexander (17). The procedure consists of using peak broadening data to calculate mean crystallite size from the Scherrer equation:

$$D = \frac{K\lambda}{\beta \cos\theta} \qquad \text{(A-1)}$$

where D is the mean crystallite size and K is a constant that depends on crystallite shape and size distribution. The value of K may vary from 0.7 to 1.7 for extremes, but is usually considered to be equal to 0.9, the standard Scherrer constant. In most cases the shape and size distribution are not known, and it has been shown that a relatively small error is introduced by setting K equal to 0.9 for most materials.

In halloysite there are two distinct (00ℓ) reflections and several (hk) two-dimensional lattice reflections, which fall off abruptly on the low-angle side and trail off gradually on the high-angle side. The size of a two-dimensional layer in the plane of the layer can be calculated by the Scherrer equation but with K = 1.84.

In the diffraction pattern of halloysite taken at $\frac{1}{8}^{\circ}$ 2θ per minute, the (hk) reflections trailed off so slowly that obtaining accurate values of peak breadth was not possible. Therefore, two determinations were made using the (001) and (002) reflections.

The mean crystallite size was considered to be the average of the two determinations. The mean crystallite size was 193 Å for hydrated halloysite and 180 Å after heating to 100°C.

As an illustration, a calculation is shown using the (001) reflection:

$2\theta = 9.34^{\circ}$

$\theta = 4.67^{\circ}$; $\tan\theta = 0.081$

$B_o = 0.600^{\circ}$, from halloysite pattern

$b = 0.074^{\circ}$, from silicon standard pattern, Figure 15

$\Delta = \frac{360}{\pi} \frac{(K\alpha_1 - K\alpha_2)}{\lambda^2_{avg}} \tan\theta_{avg}$, Δ = correction for Kα doublet separation

$\Delta = 0.0223$

$\frac{\Delta}{B_o} = 0.037$

$\frac{\Delta}{B_o} = 0.99$, from Figure 16; $B = 0.594$

$\frac{b}{B} = 0.125$

$\frac{\beta}{B} = 0.88$, from Figure 17; $\beta = 0.523^{\circ}$ or 0.009 radians

$K = 0.9$, the Scherrer constant

$D = \frac{K\lambda}{\beta \cos\theta} = 156$ Å

In addition to crystallite size effects, the presence of strain in a material will also contribute to peak broadening. The derived value, β, is actually a function of size and strain and can be used to determine the strain by the relation

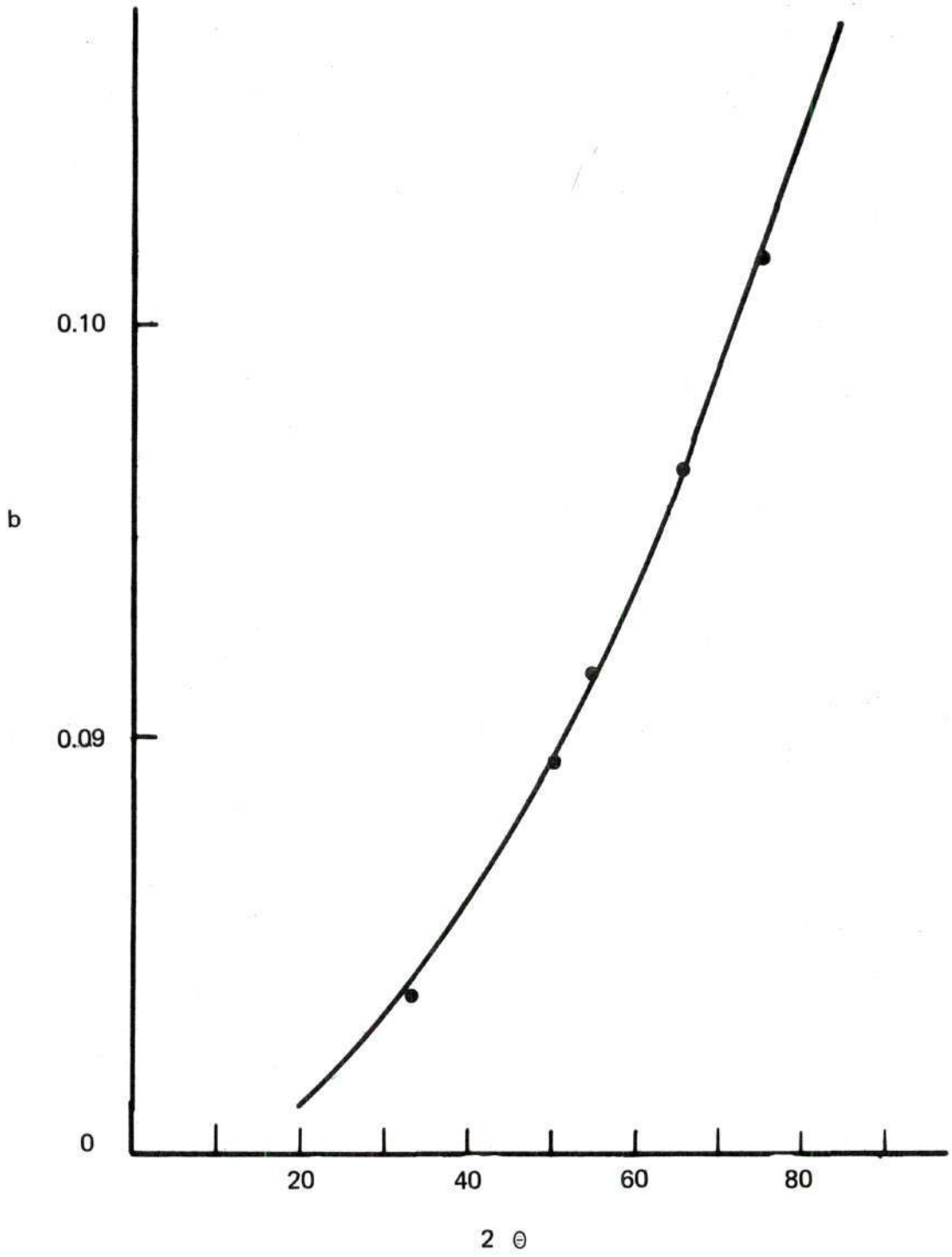

Figure 15. Instrumental Broadening as a Function of Scattering Angle.

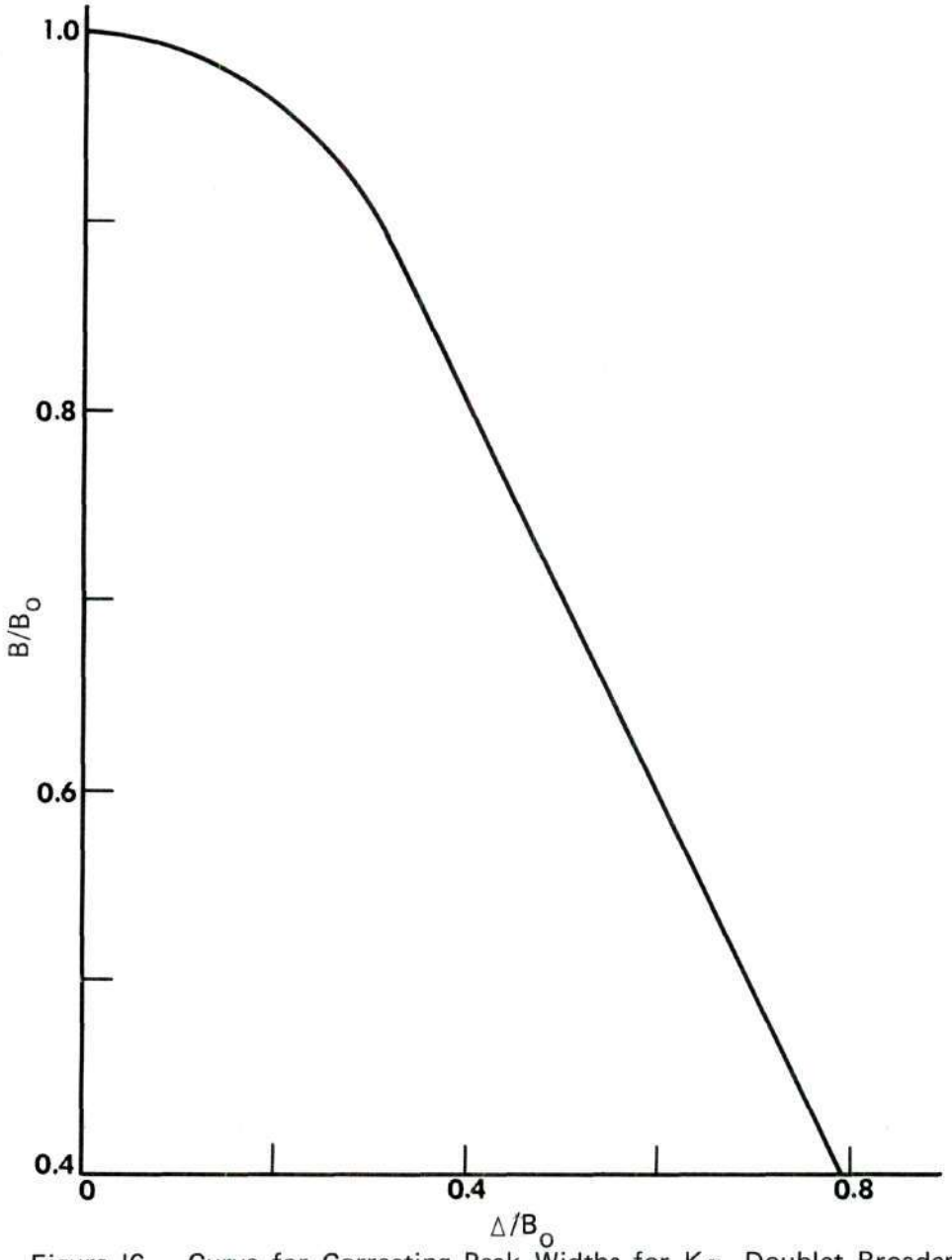

Figure 16. Curve for Correcting Peak Widths for Kα Doublet Broadening.

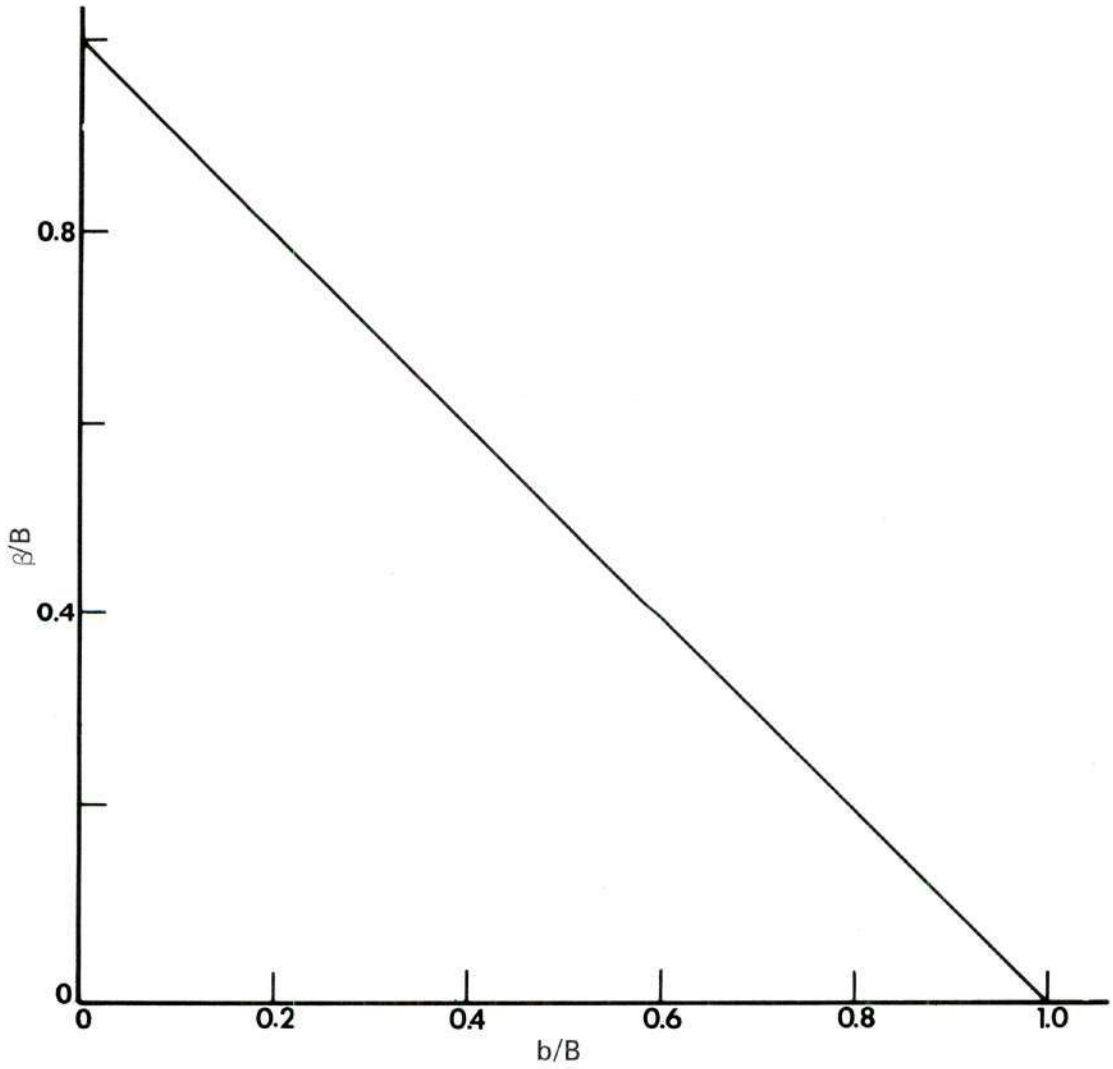

Figure 17. Curve for Correcting Peak Widths for Instrumental Broadening.

$$\beta = 2 \epsilon \tan\theta \qquad \text{(A-2)}$$

The relative contributions of crystallite size and strain may be shown in a plot of $\beta \cos\theta$ versus $\sin\theta$ (17). If the peak broadening is due to strain, the graph should be a vertical line. The intersection of the ordinate axis is a relative measure of the crystallite size. A horizontal line indicates broadening was due only to crystallite size. Intermediate slopes indicate a combination of both effects. Since there were only two data points, the results cannot be interpreted quantitatively. However, as shown in Figure 18, the data do suggest that the strain was insignificant.

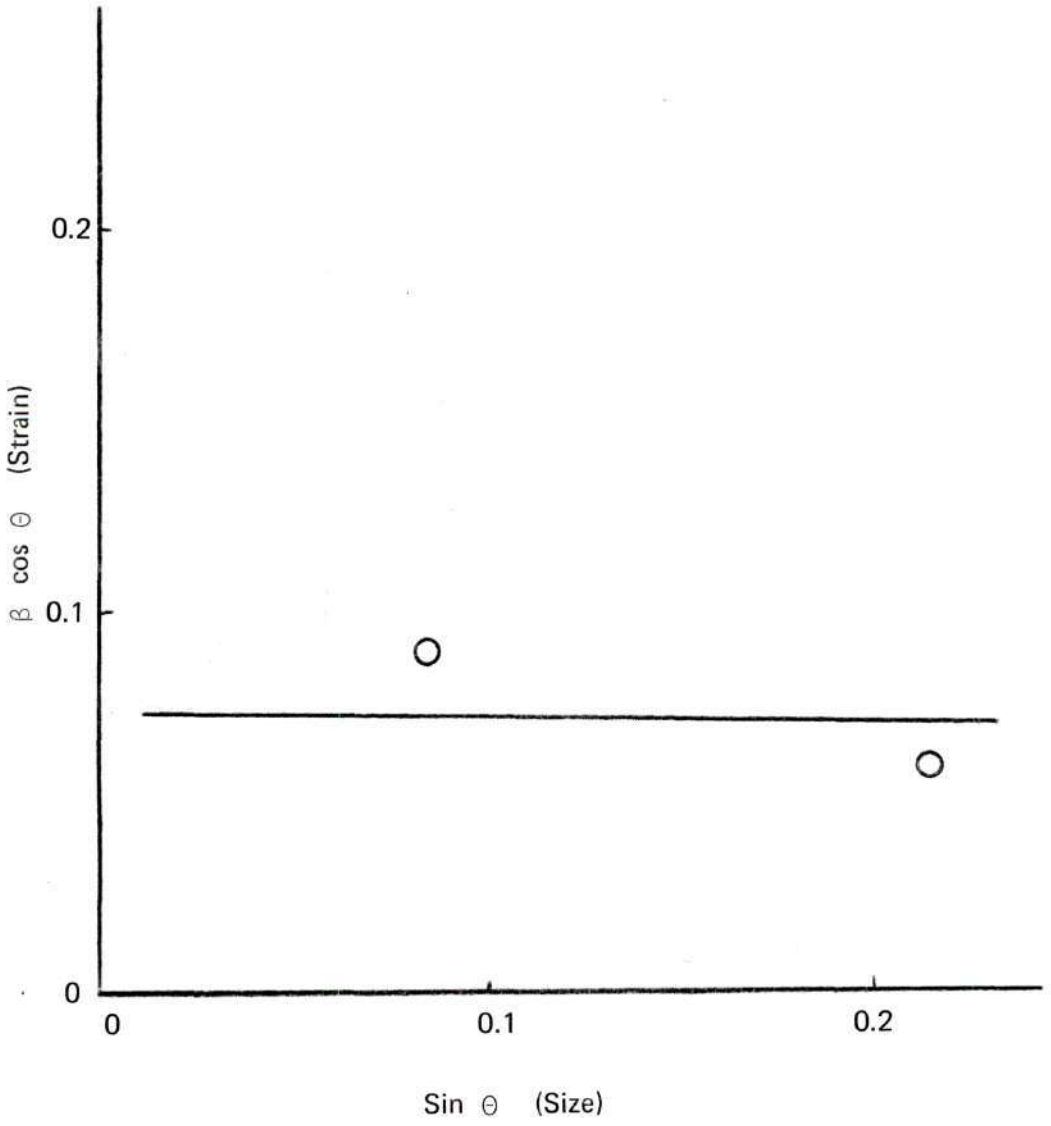

Figure 18. Contributions to Peak Broadening.

APPENDIX B

X-RAY DIFFRACTION

An indication of the structure and degree of crystallinity can be most conveniently found by x-ray diffraction analysis. The intensity and sharpness of diffraction peaks offer a means of comparison by which the effects of dehydration on the structure can be observed.

Atomic spacing values were obtained utilizing a Hull-Debye-Scherrer powder camera. Observed d-spacings were compared with calculated values and confirmed by values obtained from diffractometer traces. Table 3 gives the data obtained, along with the reference values of A.S.T.M and the American Petroleum Institute.

Table 3. X-Ray Diffraction Data for Halloysite

	Hydrated Halloysite		Halloysite		A.P.I.		A.S.T.M.	
hkℓ		I/I_o	d	I/I_o	d	I/I_o	d	I/I_o
00ℓ	10.1	100	7.37	89	7.4	98	7.4	98
02,11	4.42	70	4.42	100	4.4	100	4.41	100
002			3.61	62	3.62	63	3.62	65
003	3.36	40						
20,13	2.56	30	2.55	25	2.58	30	2.58	30
?			2.52-2.50	25	2.52-2.49	33	2.52-2.49	33
?	2.37	20						
003			2.37-2.32	27	2.39-2.32	35	2.39-2.32	35
04,22	2.23	15						
?			2.08	13			2.06	10
24,31	1.68	10	1.69-1.67	15	1.70-1.67	20	1.70-1.67	20
33,06	1.48	30	1.48	20	1.48	15	1.48	20

APPENDIX C

NEUTRON DIFFRACTION

Transmission of the Neutron Beam

Transmission measurements were made at $2\theta = 0$ for samples at room temperature and heated for one hour at 50, 100, 150, 200, and 300°C. Background corrections were made by counting neutrons that passed through a 0.457 mm cadmium sheet.

The relative transmission is the ratio of intensity with the sample in place to the intensity of the unobstructed beam. From this ratio, an attenuation coefficient, μR, can be calculated from

$$\frac{I}{I_o} = e^{-2\mu R} \qquad \text{(C-1)}$$

where I = intensity with sample in place

I_o = intensity of unobstructed beam

μR = attenuation coefficient

The values of μR obtained were then used to calculate the multiple scattering coefficient for each particular temperature. The relative transmission ratios and attenuation coefficients are shown in Table 4.

Multiple Scattering

When a neutron is incident upon a sample, it may be diffracted into the detector and counted, or it may be diffracted again within the sample,

Table 4. Neutron Diffraction Data for Hydrated Halloysite

Temp. (°C)	I/I_o	μR	δ	Multiple Scattering (%)	Multiple Scattering (neutron counts)
Ambient	0.714	0.169	0.175	18.21	326
50	0.738	0.152	0.152	15.22	256
100	0.751	0.143	0.144	14.41	201
150	0.772	0.129	0.133	13.26	182
200	0.787	0.119	0.121	12.09	161
300	0.816	0.102	0.109	10.87	90

Background Corredtion: 108 counts

if it strikes a particle in a diffraction orientation. Such secondary and subsequent orders of scattering result in a redistribution of scattering intensities and produce diffuse scattering which adds to the background of the diffraction pattern.

The background is composed of multiple scattering, hydrogen incoherent scattering, and thermal diffuse scattering. For the angular range used in the hydrogen content analysis, the thermal diffuse scattering was considered negligible. The hydrogen incoherent scattering increases exponentially with $\sin^2\theta$, while the multiple scattering can be considered constant and independent of the diffraction angle. Therefore, multiple scattering measurements were made at $2\theta = 0$. Calculations were made by the method proposed by Blech and Averbach (16).

The cross section for multiple scattering, σ_{ms}, can be calculated from

$$\sigma_{ms} = \frac{\sigma_s \, (\sigma_s/\sigma_T) \, \delta}{1 - \sigma_s/\sigma_T \, \delta} \qquad \text{(C-2)}$$

where

σ_s = scattering cross section

σ_a = absorption cross section

$\sigma_T = \sigma_s + \sigma_a$

δ = coefficient of multiple scattering

From Table 2 it is seen that σ_a is negligible and equation (C-2) reduces to

$$\sigma_{ms} = \frac{\delta}{1 - \delta} \, \sigma_s \qquad \text{(C-3)}$$

Since the hydrogen incoherent scattering is so large, the total scattering cross section can be approximated by

$$\sigma_s = n_H \sigma_H^{inc} \qquad \text{(C-4)}$$

where n_H is the number of hydrogen nuclei in the sample.

The ratio of multiple scattering, σ_{ms}, to the total scattering, σ_s, was calculated to be 0.195 for halloysite at room temperature. The multiple scattering contribution to the total diffuse background is then 18.21 percent at $2\theta = 0$. This effect is shown in Figure 19 along with the contribution of the instrumental background. The multiple scattering contributions for each sample preparation temperature are given in Table 4.

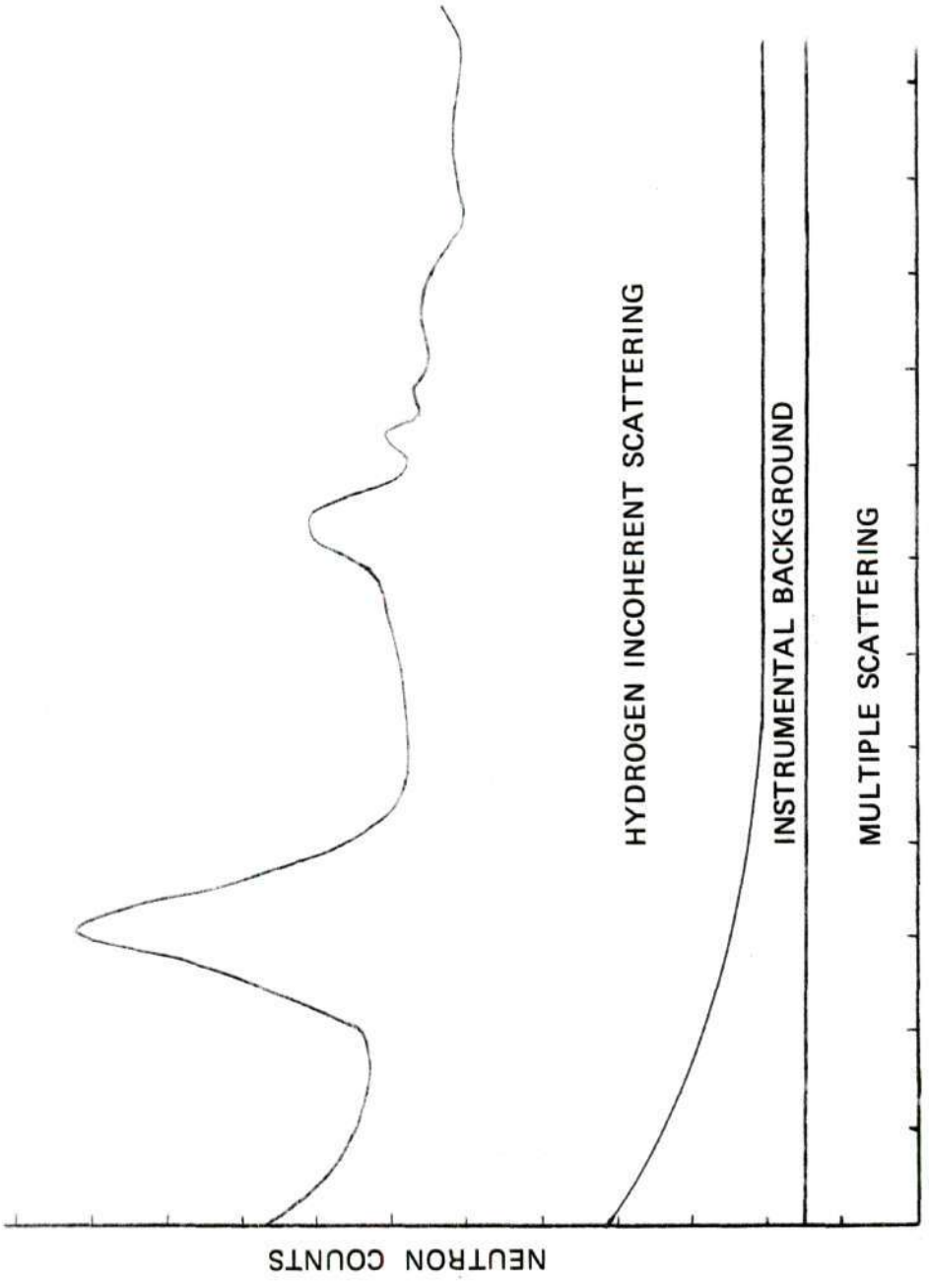

Figure 19. Contributions to the Total Diffuse Background.

BIBLIOGRAPHY*

1. Berthier, P., "Analyse de l'halloysite," Ann. Chim. Phys., 32, 332-335 (1826).

2. Meller, J. W., "A Note on the Nomenclature of Clays," Trans. English Ceramic Soc., 8, 23-30 (1908).

3. Ross, C. S. and Kerr, P. F., "Halloysite and Allophane," U. S. Geological Survey, Professional Papers, 185-G, 135-148 (1934).

4. Shaw, B. T. and Humbert, R. P., "Electron Micrographs of Clay Minerals," Soil Sci. Soc. Amer. Proceedings, 6, 146-149 (1941).

5. Bates, T. F., Hildebrand, F. A., and Swineford, A., "Morphology and Structure of Endellite and Halloysite," Amer. Mineralogist, 35, 463-484 (1950).

6. Bates, T. F. and Comer, J. J., "Electron Microscopy of Clay Surfaces" in Clays and Clay Minerals, National Academy of Science--National Research Council Publication 395, 1-25, 1955.

7. Brindley, G. W. and Robinson, K., "X-Ray Studies of Halloysite and Metahalloysite, Part I: The Structure of Metahalloysite, an Example of a Random Layer Lattice," Mineralogy Magazine, 28, 393-406 (1948).

8. Brindley, G. W., Santos, P., and Santos, H., "Mineralogical Studies of Kaolinite-Halloysite Clays, Part I: Identification Problems," Amer. Mineralogist, 48, 897-909 (1963).

9. Hendricks, S. B., "On the Structure of the Clay Minerals: Dickite, Halloysite, and Hydrated Halloysite," Amer. Mineralogist, 23, 295-301 (1938).

10. Grim, R. E., "Clay Mineralogy," McGraw-Hill Book Co., New York, 70-76, 126-135, 1968.

11. Pauling, L. C., "The Structure of Micas and Related Minerals," National Academy of Science Proceedings, 16, 123-129 (1930).

12. Brindley, G. W., "Structural Mineralogy of Clays," Clays and Clay Technology Bulletin 169, California Dept. of Natural Resource, Div. of Mines, 33-42, 1955.

---

*Abbreviations follow the form used by Chemical Abstracts (1965).

BIBLIOGRAPHY (Concluded)

13. Brindley, G. W. and Goodyear, J., "X-Ray Studies of Halloysite and Metahalloysite, II: The Transition of Halloysite to Metahalloysite in Relation to Relative Humidity," Mineralogy Mag., 28, 203-215 (1948).

14. Grim, R. E. and Bradley, W. F., "Rehydration and Dehydration of the Clay Minerals," Amer. Mineralogist, 33, 50-59 (1948).

15. Bacon, G. E., "Neutron Diffraction," Monographs on the Physics and Chemistry of Materials, Oxford University Press, London, 1962.

16. Blech, I. A. and Averbach, B. L., "Multiple Scattering of Neutrons in Vanadium and Copper," Phys. Rev., 137, A1113-A1116 (1965).

17. Klug, H. P. and Alexander, L. E., "X-Ray Diffraction Procedures," John Wiley and Sons, Inc., New York, 1966.